US Department
of Transportation

**Federal Railroad
Administration**

Propagation Analysis of Transverse Defects Originating at the Lower Gage Corner of Rail

Office of Research and
Development
Washington, DC 20590

D.Y. Jeong
Y.H. Tang
O. Orringer
A.B. Perlman

U.S. Department of Transportation
Research and Special Programs Administration
Volpe National Transportation Systems Center
Cambridge, Massachusetts 02142

DOT/FRA/ORD-98/06
DOT-VNTSC-FRA-98-14

December 1998
Final Report

REPORT DOCUMENTATION PAGE

Form Approved
OMB No. 0704-0188

1. AGENCY USE ONLY (Leave blank)	2. REPORT DATE	3. REPORT TYPE & DATES COVERED
	December 1998	Final Report - June 1996

4. TITLE AND SUBTITLE
Propagation Analysis of Transverse Defects Originating at the Lower Gage Corner of Rail

5. FUNDING NUMBERS
R9002/RR928

6. AUTHOR(S)
David Y. Jeong,[1] Yim H. Tang,[1] O. Orringer,[1,2] and A. Benjamin Perlman [1,2]

7. PERFORMING ORGANIZATION NAME(S) AND ADDRESS(ES)
[1] U.S. Department of Transportation
Research and Special Programs Administration
Volpe National Transportation Systems Center
Cambridge, MA 02142-1093

[2] Tufts University
Mechanical Engineering Department
Medford, MA 02155

8. PERFORMING ORGANIZATION REPORT NUMBER
DOT-VNTSC-FRA-98-14

9. SPONSORING/MONITORING AGENCY NAME(S) AND ADDRESS(ES)
U.S. Department of Transportation
Federal Railroad Administration
Office of Research and Development
Washington, DC 20590

10. SPONSORING OR MONITORING AGENCY REPORT NUMBER
DOT/FRA/ORD-98/06

11. SUPPLEMENTARY NOTES

12a. DISTRIBUTION/AVAILABILITY
This document is available to the public through the National Technical Information Service, Springfield, VA 22161. This document is also available on the FRA web site at www.fra.dot.gov.

12b. DISTRIBUTION CODE

13. ABSTRACT (Maximum 200 words)
This report describes analyses performed to examine the growth rate of a particular transverse defect that forms in the rail head. The most common transverse defect found in rail, known as the detail fracture, has been studied in previous work. The present analyses, however, focuses on another internal transverse defect which originates at the lower gage corner of the rail head and has not been examined previously. This defect has been provisionally named “reverse detail fracture” because its origin is in the lower gage corner rather than the upper gage corner where detail fractures have been known to occur. The growth rate of reverse detail fractures is examined by modifying a model previously developed to analyze detail fractures. These modifications and other details of the analyses are described in this report. Using this model, sensitivity studies were conducted to examine the effect of various service conditions on the propagation life of reverse detail fractures. In addition, an approximate method to examine the effect of wear on rail stresses is described in this report. Wear is assumed to occur by a uniform loss of material from either the top of the rail or from the gage-side face. The approximate method is used to examine the effect of wear on propagation life. The results of the analyses indicate that the safe crack-growth life of reverse detail fractures is about 20% shorter than that for ordinary detail fractures under the same conditions. This suggests that the inspection interval should be reduced for rails where reverse detail fractures are expected to occur. The results also indicate that residual stress, thermal tension, and wear have a relatively strong influence on reducing the safe crack-growth life of reverse detail fractures.

14. SUBJECT TERMS	15. NUMBER OF PAGES
crack propagation, critical defect size, detail fracture, fracture mechanics, reverse detail fracture, safe crack-growth life, transverse defect	60
	16. PRICE CODE

17. SECURITY CLASSIFICATION OF REPORT	18. SECURITY CLASSIFICATION OF THIS PAGE	19. SECURITY CLASSIFICATION OF ABSTRACT	20. LIMITATION OF ABSTRACT
Unclassified	Unclassified	Unclassified	

PREFACE

In support of the Federal Railroad Administration's (FRA) Track Safety Research Program, the John A. Volpe National Transportation Systems Center (Volpe Center) has been conducting and managing research to develop technical information that can be used to support rational criteria for the preservation of safe operations on railroad tracks.

The crack propagation life of transverse defects known as detail fractures has been examined in previous research conducted by the Volpe Center. Recently, however, another type of internal transverse defect has been discovered during inspections of revenue track. This defect has been provisionally named "reverse detail fracture" because its origin is at the lower gage corner of the rail head rather than at the upper gage corner, where detail fractures are known to occur.

The growth rate of reverse detail fractures is examined by modifying a model previously developed to analyze detail fractures. These modifications and other details of the analyses are described in this report. Using this model, sensitivity studies were conducted to examine the effect of various service conditions on the propagation life of reverse detail fractures. In addition, an approximate method to examine the effect of wear on rail stresses is described in this report. Wear is assumed to occur by a uniform loss of material from either the top of the rail or from the gage-side face. The approximate method is used to examine the effect of wear on propagation life.

The results of the analyses indicate that the safe crack-growth life of reverse detail fractures is about 20% shorter than that for ordinary detail fractures under the same conditions. This suggests that the inspection interval should be reduced for rails in which reverse detail fractures are expected to occur. The results also indicate that residual stress, thermal tension, and wear have a relatively strong influence on reducing the safe crack-growth life of reverse detail fractures.

METRIC/ENGLISH CONVERSION FACTORS

ENGLISH TO METRIC	METRIC TO ENGLISH
LENGTH (APPROXIMATE)	**LENGTH (APPROXIMATE)**
1 inch (in) = 2.5 centimeters (cm)	1 millimeter (mm) = 0.04 inch (in)
1 foot (ft) = 30 centimeters (cm)	1 centimeter (cm) = 0.4 inch (in)
1 yard (yd) = 0.9 meter (m)	1 meter (m) = 3.3 feet (ft)
1 mile (mi) = 1.6 kilometers (km)	1 meter (m) = 1.1 yards (yd)
	1 kilometer (km) = 0.6 mile (mi)
AREA (APPROXIMATE)	**AREA (APPROXIMATE)**
1 square inch (sq in, in^2) = 6.5 square centimeters (cm^2)	1 square centimeter (cm^2) = 0.16 square inch (sq in, in^2)
1 square foot (sq ft, ft^2) = 0.09 square meter (m^2)	1 square meter (m^2) = 1.2 square yards (sq yd, yd^2)
1 square yard (sq yd, yd^2) = 0.8 square meter (m^2)	1 square kilometer (km^2) = 0.4 square mile (sq mi, mi^2)
1 square mile (sq mi, mi^2) = 2.6 square kilometers (km^2)	10,000 square meters (m^2) = 1 hectare (ha) = 2.5 acres
1 acre = 0.4 hectare (he) = 4,000 square meters (m^2)	
MASS - WEIGHT (APPROXIMATE)	**MASS - WEIGHT (APPROXIMATE)**
1 ounce (oz) = 28 grams (gm)	1 gram (gm) = 0.036 ounce (oz)
1 pound (lb) = 0.45 kilogram (kg)	1 kilogram (kg) = 2.2 pounds (lb)
1 short ton = 2,000 pounds (lb) = 0.9 tonne (t)	1 tonne (t) = 1,000 kilograms (kg)
	= 1.1 short tons
VOLUME (APPROXIMATE)	**VOLUME (APPROXIMATE)**
1 teaspoon (tsp) = 5 milliliters (ml)	1 milliliter (ml) = 0.03 fluid ounce (fl oz)
1 tablespoon (tbsp) = 15 milliliters (ml)	1 liter (l) = 2.1 pints (pt)
1 fluid ounce (fl oz) = 30 milliliters (ml)	1 liter (l) = 1.06 quarts (qt)
1 cup (c) = 0.24 liter (l)	1 liter (l) = 0.26 gallon (gal)
1 pint (pt) = 0.47 liter (l)	
1 quart (qt) = 0.96 liter (l)	
1 gallon (gal) = 3.8 liters (l)	
1 cubic foot (cu ft, ft^3) = 0.03 cubic meter (m^3)	1 cubic meter (m^3) = 36 cubic feet (cu ft, ft^3)
1 cubic yard (cu yd, yd^3) = 0.76 cubic meter (m^3)	1 cubic meter (m^3) = 1.3 cubic yards (cu yd, yd^3)
TEMPERATURE (EXACT)	**TEMPERATURE (EXACT)**
[(x-32)(5/9)] °F = y °C	[(9/5) y + 32] °C = x °F

QUICK INCH - CENTIMETER LENGTH CONVERSION

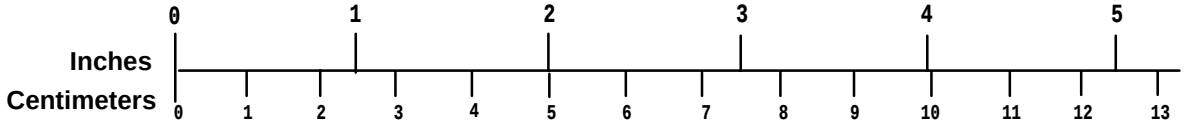

QUICK FAHRENHEIT - CELSIUS TEMPERATURE CONVERSION

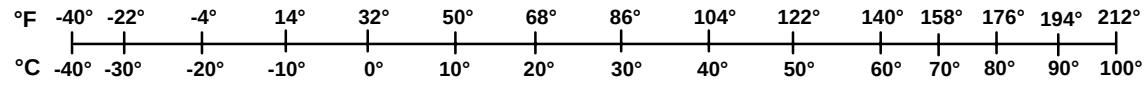

For more exact and or other conversion factors, see NIST Miscellaneous Publication 286, Units of Weights and Measures. Price $2.50 SD Catalog No. C13 10286

Updated 6/17/98

TABLE OF CONTENTS

Section **Page**

1. INTRODUCTION 1

2. MODEL FOR REVERSE DETAIL FRACTURES 5

2.1 Stress Analysis 5

2.1.1 Bending Stresses 5
2.1.2 Residual Stresses 6
2.1.3 Thermal Stresses 7

2.2 Crack Geometry Effects 8

2.2.1 Finite Cross-Section 8
2.2.2 Non-Uniform Stress 9

2.3 Life Calculation 12

2.4 Analysis for Worn Rail 13

2.4.1 Loss of Rail-Head Height 15
2.4.2 Loss of Rail-Head Width 19

3. SENSITIVITY STUDIES 23

3.1 Effect of Wear 23
3.2 Effect of Thermal Stress 26
3.3 Effect of Residual Stress 28
3.4 Effect of Rail Size 28
3.5 Effect of Track Curvature 31
3.6 Effect of Dynamic Load Factor 31
3.7 Effect of Foundation Stiffness 33
3.8 Summary of Sensitivity Studies 35
3.9 Comparison with Detail Fracture 38

4. CONCLUSIONS 41

REFERENCES 43

APPENDIX A. Equations for Rail-Bending Stresses 45
APPENDIX B. Equations for Section Properties of Worn Rail 51

LIST OF FIGURES

Figure		Page
1.	RDF Defect in Lower Gage Corner of the Rail Head	3
2.	Stress Cycles Produced from Adjacent Ends of Coupled Hopper Cars	6
3.	Residual Stress in Rail Head as a Function of RDF Size	7
4.	Schematic of Quarter-Circular Crack at Lower Gage Corner of the Rail Head	8
5.	Actual and Idealized Rail Cross-Sections	13
6.	Idealized Rail-Head Wear Patterns	14
7.	Schematic for Vertical Bending Inertia Calculation for Rail-Head Height Loss	15
8.	Schematic of Lateral Bending Inertia Calculation for Rail with Head-Width Loss	19
9.	Schematic of Vertical Bending Inertia Calculation for Rail with Head-Width Loss	20
10.	Effect of Wear Pattern on RDF Growth	24
11.	Effect of Head-Height Loss on RDF Safe Crack-Growth Life	25
12.	Effect of Head-Height Loss on Critical RDF Size	25
13.	Effect of Thermal Tension on RDF Safe Crack-Growth Life	27
14.	Effect of Thermal Tension on Critical RDF Size	27
15.	Effect of Residual Stress Severity Level on RDF Safe Crack-Growth Life	29
16.	Effect of Residual Stress Severity Level on Critical RDF Size	29
17.	Effect of Rail Size on RDF Safe Crack-Growth Life	30
18.	Effect of Rail Size on Critical RDF Size	30
19.	Effect of Track Curvature on RDF Safe Crack-Growth Life	32
20.	Effect of Track Curvature on Critical RDF Size	32
21.	Effect of Dynamic Load Factor on RDF Safe Crack-Growth Life	34
22.	Effect of Dynamic Load Factor on Critical RDF Size	34
23.	Effect of Foundation Stiffness on RDF Safe Crack-Growth Life	36
24.	Effect of Foundation Stiffness on Critical RDF Size	36
25.	Summary of RDF Results for Safe Crack-Growth Life	37
26.	Summary of Results for Critical RDF Defect Sizes	37
27.	Comparison between DF and RDF Defect Growth	39
28.	Effect of Head-Height Loss on DF Growth Rate	39
A-1.	Dimensions for a Generic Rail Section	46
A-2.	Eccentric Vertical Loading and Lateral Loading of Rail	49
B-1.	Shear Center and Centroid Locations for Rail with Reduced Head Width	54

LIST OF TABLES

Table **Page**

1. Finite-Section Magnification Factors for Various RDF Sizes in Unworn Rail 9
2. Stress-Gradient Magnification Factors for Unworn 132 RE Rail Section (P=4) .. 11
3. Estimated Section Properties for 132 RE Rail with Loss of Head Height 16
4. Finite-Section Magnification Factors for Worn Rail 17
5. Stress-Gradient Magnification Factors for 132 RE Rail Section with Loss of Head Height (P=4) 18
6. Estimated Section Properties for 132 RE Rail with Loss of Rail-Head Width 20
7. Stress-Gradient Magnification Factors for 132 RE Rail Section with Loss of Head Width (P=4) 21
8. Baseline Parameters for Sensitivity Studies 23
9. Tensile Thermal Stress for Various Temperature Differences 26
10. Load Descriptions for Varying Track Curvature 31
11. Representative Vertical Foundation Moduli 33

EXECUTIVE SUMMARY

This report is essentially an extension of previous work conducted in support of rail integrity research. Previous research focused on studying a particular type of defect called a “detail fracture.” Detail fractures are the most prevalent rail defects in continuous welded rail (CWR) tracks carrying heavy-weight, high-density train traffic. A significant product of rail integrity research was the development of an analytical model to predict the growth rate of detail fractures under revenue service conditions. The model was used later to provide guidelines for rail inspection frequencies.

Recently, a new type of internal transverse defect has been discovered in inspections of revenue track. The origin of this defect is located at the lower gage corner of the rail head rather than at the upper gage corner, where detail fractures usually initiate. For this reason, this new type of defect has been provisionally named “reverse detail fracture.” Such defects occur in poorly lubricated, curved, worn rail on stiff track carrying traffic with high axle loads.

Nondestructive detections of internal transverse defects have been performed by the railroad industry with equipment based on the principles of ultrasound and magnetic induction. Without special attention, however, the distinction between detecting detail fractures and reverse detail fractures can be overlooked. Even if these defects can be distinguished by rail-testing equipment, the only reliable method to confirm the result would be to remove the rail section from revenue service and break it open. This report describes analyses of reverse detail fractures to determine whether inspection intervals should be adjusted accordingly.

The analysis of reverse detail fractures was performed by modifying the model originally developed to analyze detail fractures. The modifications were required to account for the differences in geometry between these defects. Sensitivity studies were conducted using the model for reverse detail fractures to examine the relative effect of various service conditions on the safe crack-growth life. These service conditions included residual stress, thermal tension, wear, rail size, track curvature, dynamic load factor, and foundation stiffness.

The effect of wear was examined by assuming two different geometric patterns. One pattern assumed uniform loss of material from the top of the rail head, which results in reduced rail-head height. The other pattern assumed uniform loss of material from the gage-side face. An approximate method was developed to determine the rail section properties used in the stress analysis for worn rail. This approximate method was applied to determine the propagation life of transverse defects in worn rail.

Results from the model suggest that loss of head height has a greater influence on reducing the safe crack-growth life of reverse detail fractures than an equivalent reduction in head width, in terms of percentage of worn head area.

Results of the sensitivity studies reveal that residual stress, thermal tension, and wear have the strongest effect on reducing the safe crack-growth life of reverse detail fractures. Foundation stiffness has a relatively weak effect on reducing safe life.

Moreover, the results presented in this report indicate that, although reverse detail fractures and ordinary detail fractures initially grow at somewhat comparable rates, the safe crack-growth life of the reverse detail fracture is 20% less than that of a detail fracture under the same conditions. This result suggests that inspection frequency should be increased for rails in which reverse detail fractures are expected to occur.

1. INTRODUCTION

Transverse defects in rail usually originate beneath the running surface on the gauge side. The most prevalent transverse defect in continuous welded rail (CWR) is known as the detail fracture (DF). Such defects have been analyzed extensively in previous studies [1] – [4].

In support of the Federal Railroad Administration's (FRA) Track Safety Research Program, an analysis model was developed [5] to facilitate consistent and realistic estimates of the safe crack-growth life[1] for detail fractures under representative service conditions. Consistency in the estimation of safe crack-growth life was achieved by basing the model on the combination of beam-theory stresses and established crack stress intensity factor ("K") formulas from engineering fracture mechanics.[2] The detail fracture was modeled with two basic "K" formulas: one for a circular crack embedded in an unbounded body to represent defects up to 50% HA, and one for a quarter-circular surface crack in an unbounded quarter-space body to represent larger defects that have broken out to the gauge face and/or running surface. The basic "K" formulas were modified with empirical factors to represent the non-circular shapes of typical detail fractures before breakout and to account for the finite dimensions of the rail cross-section. Realism was achieved by comparing the model predictions with the results of laboratory and field tests. The laboratory tests were conducted mainly to establish a quantitative relation between "K" and the rate of crack growth in typical rail steels. The field tests, most of which were conducted by the Transportation Technology Center on the Facility for Accelerated Service Testing (FAST), allowed the model to be refined by comparing predictions of DF life with the measured behavior of actual defects that were subjected to FAST train loads. The model was validated by requiring that its crack-growth life predictions agree with the FAST test results when the inputs reflected the FAST test conditions and the laboratory "K" versus growth rate measurements. Reference [5] is a comprehensive description of the model, laboratory test results, field test results, and initial validation based on the growth of detail fractures in tangent track. The model was further validated with subsequent field tests of detail fracture growth on curved track [8].[3]

Recently, a new type of transverse defect in the rail head has been reported from inspections of revenue track. The defect type has been provisionally named "reverse detail fracture" (RDF). RDF defects occur in poorly lubricated, curved, worn rail on stiff track carrying traffic with high average axle loads. Some of these defects are associated with either thermite or flash-butt welds, but as many or more are found away from rail ends. The origin of the defect is the lower gauge corner, generally in or near a flow lip with a notch in the lip. The defect has an immediate orientation in the transverse

---

[1] "Safe crack-growth life" as used here means the unfactored estimate of gross tons over the track, from the time at which the defect has become just large enough to be detectable, to the time at which the defect has grown just large enough to cause a rail failure under the next train.

[2] Stress intensity factor formulas for a variety of crack configurations can be found in handbooks such as References [6] and [7].

[3] This latter validation [8] required a minor change in the way that rail residual stress is modeled for detail fractures smaller than 10% HA.

plane, and the propagation surface is much more nearly flat than the surface of a typical detail fracture. A typical RDF defect is shown in Figure 1. The photograph shows a 132 RE section in which approximately 30 to 40% of the rail head area has been lost to wear.

After the discovery of the RDF defect was reported to FRA, the Volpe National Transportation Systems Center (Volpe Center) began conducting analyses to determine the safe crack-growth life of these defects. The RDF analyses and their results are described in this report. The analyses were performed by modifying the existing model for detail fractures to account for the differences in geometry between the RDF and DF defects. The analyses included sensitivity studies performed to examine the effect of various service conditions on RDF crack growth. The following conditions were evaluated in the sensitivity studies: foundation stiffness, track curvature, rail section, neutral and service temperatures for continuous welded rail (CWR), and dynamic load factor.[4] The effect of residual stresses in the rail head was also examined in these sensitivity studies. The analyses also included a comparison between the crack growth rates of RDF defects and detail fractures.

In addition to propagation analyses, an approximate method to account for rail wear is described in this report. Wear is assumed to occur from uniform loss of material from either the top of the rail, which results in head-height loss, or from the gage side of the rail resulting in a reduced rail-head width. The method estimates the section properties required in the beam-theory stress analysis of the rail in bending. The growth rates of RDF defects in worn rail were analyzed using this approximate method.

Section 2 describes the model for RDF defects, as modified from the previously developed model for detail fractures. Specific details are discussed in this section involving the stress analysis, crack geometry effects, the calculation for safe crack-growth life, and the approximate method of analyzing worn rail.

Section 3 presents results from the sensitivity studies performed to examine the influence of various service conditions on the RDF safe crack-growth life and critical RDF size.[5] The results from the comparison between the growth rates of RDF and DF defects are also presented in this section.

Finally, Section 4 discusses the results and provides conclusions drawn from the analyses described in this report.

[4] The model developed for detail fractures includes the capability to analyze the effect of train makeup. A simplified load spectrum was used in the model for RDF defects, and is described in Section 2.1.

[5] "Critical" defect size is the predicted flaw size at which a rail with average properties in terms of fracture resistance is expected to fail under the next train passage.

2. MODEL FOR REVERSE DETAIL FRACTURES

The detail fracture model developed in Orringer, et al., [5] was modified in this study to evaluate the safe crack-growth life for RDF defects. These modifications addressed geometric differences between the RDF and DF defects. Based on the corner origin of the typical RDF (Figure 1), only the post-breakout part of the DF model was applied to analyze RDF defects. Thus, the quarter-circular "K" formula was the basis for the RDF analysis. Another minor change was required to relocate the center of the quarter-circle from the vicinity of upper gauge corner (representing a DF) to the lower gauge corner for the RDF defect.

Details of the RDF model are described in this section. Specifically, the stress analysis, the life calculation, and the methodology developed to analyze worn rail are described.

2.1 STRESS ANALYSIS

Fatigue crack growth is driven by cyclic loading produced by repeated wheel loading. Stress cycles are created from bending of the rail as trains travel over the track. The RDF defect model considers only the longitudinal component of stress because this component, when tensile, is associated with opening the crack, which leads to crack growth. In addition to bending, however, residual stresses and temperature differences from the stress-free (or neutral) temperature also contribute to the overall magnitude of the longitudinal stress. In the stress analysis for transverse defects, the state of stress at a given point in the rail and for a given defect size is simply the sum of the bending, residual, and thermal stresses in the longitudinal direction.

2.1.1 Bending Stresses

The stresses produced by bending of the rail were calculated using an analysis originally developed by Timoshenko and Langer [9], which assumes the rail to behave as a continuous beam supported by elastic foundations in the vertical, lateral, and rotational directions. Moreover, the longitudinal bending stress in the rail head is assumed to comprise five components: (1) vertical bending, (2) lateral bending, (3) warping, (4) vertical head-o-web bending, and (5) lateral head-on-web bending. Timoshenko and Langer [9] derived a system of coupled differential equations to determine these various bending components. More recently, a simplified analysis, in which the differential equations were decoupled, was shown to approximate these bending stresses within reasonable engineering accuracy.[6] The results of the simplified analysis have been incorporated into the stress analysis of the crack growth models for transverse defects. The equations used to determine rail bending stresses are given in Appendix A.

Rail bending stresses were calculated for a simplified spectrum of repeated 33-ton axle loads, considered in groups of four corresponding to the adjacent ends of coupled hopper cars. The 33-ton axle loads represent those for a fully loaded, open hopper car. Figure 2 shows the variation of longitudinal stress along the rail at the lower gauge cor-

[6] The simplified Timoshenko and Langer analysis is described in References [4] and [5].

ner position, produced by the adjacent ends of coupled hopper cars. A simplified stress spectrum can be constructed from this variation of the longitudinal bending stresses, which consists of 5 cycles, or five pairs of minimum and maximum stresses.

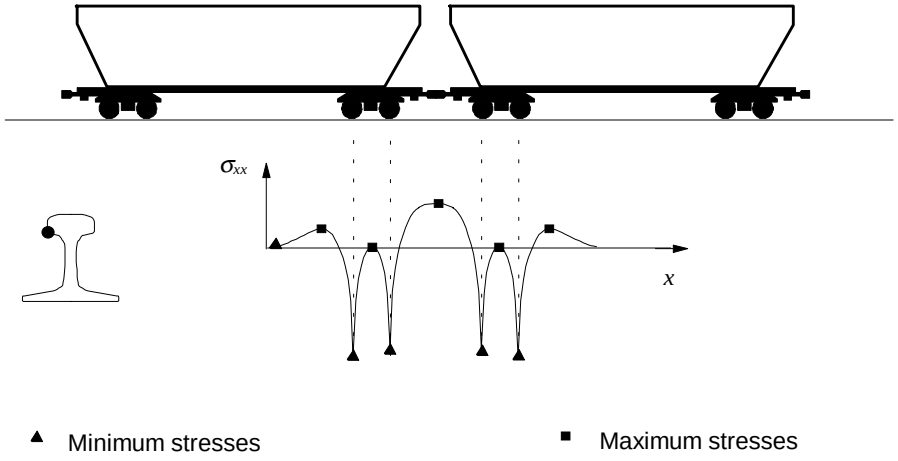

Figure 2. Stress Cycles Produced from Adjacent Ends of Coupled Hopper Cars

2.1.2 Residual Stresses

Residual stresses are those remaining in the rail when no external loads are present. Initially, residual stresses are created when the rail is quenched during the manufacturing process. Since the rail cross-section is non-uniform in the thickness direction, the rail cools non-uniformly, creating gradients in the residual stress field. Residual stresses created during initial manufacturing have been examined in [10]. Residual stresses are also created from cold working during roller straightening, which have been examined in [11]. Moreover, the magnitudes of the residual stresses are affected by the plastic deformations that occur during in-service loading. Eventually, the residual stresses stabilize to a so-called “shakedown” limit. A methodology to predict the residual stresses from service loading is described in [12].

Residual stresses have been measured in a limited number of rails obtained from revenue service [13]. Most of these data were collected from rails originally placed on tangent sections of railroad track. One section, however, was taken from a 115 RE rail on curved track [4]. The measurement of residual stresses was performed in a destructive manner; strains were measured while the rail was cut into several slices. Cutting of the rail in this manner relieved the internal or residual stresses, and strain gauges measured the strains associated with the stress relief. Contour plots of residual stress in the rail were constructed from the strain measurements based on purely elastic unloading.[7]

[7] Purely elastic unloading is a simplifying assumption that neglects the so-called Bauschinger effect. However, the distributions of axial residual stress calculated on the basis of this assumption were found to be self-equilibrating.

For computational convenience, the relation between residual stress and defect size must be known. For this purpose, defects of various sizes (i.e., quarter-circular cracks of different radii measured from the lower gauge corner to the perimeter of the flaw) were superimposed over the axial residual stress contours obtained from the curved-track rail sample. The average stress enclosed with the outline of a given defect was considered as the residual stress associated with that particular defect size. Figure 3 shows the residual stress as a function of RDF size, as determined by this procedure.

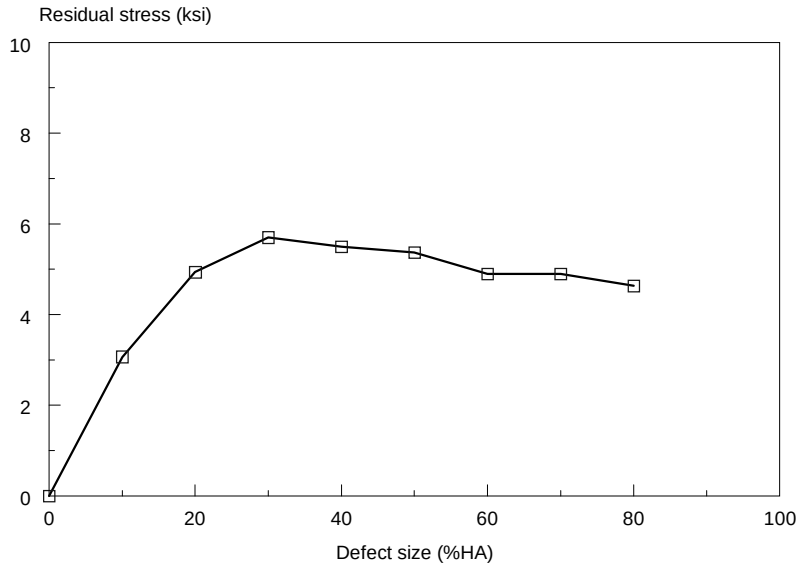

Figure 3. Residual Stress in Rail Head as a Function of RDF Size

2.1.3 Thermal Stresses

Thermal stresses are produced in continuous welded rail (CWR) when the service temperature differs from the stress-free or neutral temperature. For fully restrained CWR in tangent track, the magnitude of the thermal stress can be determined from

$$\sigma_{TH} = E\alpha(T_N - T) \tag{1}$$

where E is the modulus of elasticity, α is the coefficient of thermal expansion, T_N is the neutral or stress-free temperature, and T is the service temperature. For rail steel, E is 30×10^6 psi and α is 6.5×10^{-6} per °F. As indicated in equation (1), a service temperature below the stress-free temperature produces tensile thermal stress. The current

analyses have been simplified by assuming an average or constant temperature difference throughout the fatigue life of the RDF defect.[8]

2.2 CRACK GEOMETRY EFFECTS

The RDF defect was modeled as a quarter-circular crack in a finite body subjected to bending stresses (Figure 4). The handbook solution for the stress intensity factor associated with a quarter-infinite body was modified to account for the effects of finite boundaries and non-uniform stress. The stress intensity factor formula for the RDF defect thus has the following mathematical form

$$K_I = \frac{2}{\pi} M_1(a) M_G(a) \sigma \sqrt{\pi a} \tag{2}$$

where σ is the stress level, M_1 is the correction factor for finite boundaries, M_G is the correction factor for non-uniform stress, and a is the radius of the defect. The mathematical equations associated with these correction factors are described in the next two subsections.

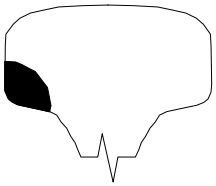

Figure 4. Schematic of Quarter-Circular Crack at Lower Gage Corner of the Rail Head

2.2.1 Finite Cross-Section

The same formula used in the detail fracture model [5] for finite cross-section is also used in the RDF model. This formula for finite boundaries is mathematically analogous to the correction factor for a through crack growing across a plate of finite width subjected to either uniform tension or bending. In the models for corner cracks in the rail head, the finite-section magnification is expressed as

$$M_1\left(\frac{A}{A_X}\right) = \sqrt{\frac{2A_X}{\pi A}\tan\left(\frac{\pi A}{2A_X}\right)} \frac{0.83 + 2.02(A/A_X) + 0.37\left[1 - \sin(\pi A / 2A_X)\right]^3}{\cos(\pi A / 2A_X)} \tag{3}$$

where $A_X = A_H + 0.5A_R$. In these equations, A is the area of the defect (in units of inches^2), A_H is the cross-sectional area of the rail head only, and A_R is the

[8] The effect of varying thermal stress (or thermal stress history) can be examined in the model if the relation between thermal stress and either defect size or tonnage is known *a priori*.

cross-sectional area of the entire rail. Thus, the finite-section magnification factor is a function of rail section. Table 1 lists the magnitude of this factor for different defect sizes and rail sections. In the limit as A approaches zero, the finite-section magnification factor approaches the value of 1.2.

Table 1. Finite-Section Magnification Factors for Various RDF Sizes in Unworn Rail

RDF Size (% HA)	Rail Size					
	70 ASCE	100 RE	115 RE	132 RE	136 RE	140 RE
10	1.222	1.221	1.219	1.219	1.220	1.220
20	1.264	1.259	1.254	1.254	1.257	1.257
30	1.325	1.316	1.306	1.304	1.311	1.310
40	1.408	1.393	1.375	1.371	1.383	1.382
50	1.514	1.490	1.462	1.457	1.475	1.474
60	1.647	1.610	1.569	1.562	1.589	1.587
70	1.809	1.758	1.699	1.689	1.728	1.725
80	2.008	1.937	1.856	1.842	1.895	1.891

2.2.2 Non-Uniform Stress

The stress intensity factor for a corner flaw varies with position along the crack front [6], [7]. The variation of the stress intensity also depends on whether the applied stress field is uniform tension or bending [14]. The variation of stress intensity factor with position along the crack front means that the aspect ratio of an elliptical flaw should change as the crack grows. This type of growth is referred to as non-self-similar crack growth. To simplify the present analysis, non-self-similar crack growth was neglected by averaging the value of the stress intensity factor along the crack front and assuming that the aspect ratio for RDF defects remains constant while the crack grows. This average value of transverse defects in the rail head is now referred to as the stress-gradient magnification factor. The method to determine this factor is described in this subsection.

As described in Section 2.1.1, five loading components contribute to the bending stress in the rail head. The two most dominant ones, which are considered in the following derivation, are vertical bending about the rail neutral axis and lateral bending about the rail center plane. The stress intensity factor for an elliptical corner flaw of aspect ratio b/a in a combined bending field with flaw center location (y, z)[9] can be expressed as

$$K_I(\theta) = \frac{2}{\pi}\sigma\sqrt{\pi a}\,M(\theta) \tag{4}$$

[9] In this derivation, the coordinates (y, z) refer to the location of the stress point relative to the centroidal axes of the rail section.

where $M(\theta)$ is a function of angle around the crack. For a corner flaw in the rail head, this function is given in Orringer, et al. [5], as

$$M(\theta) = \frac{M_v(\theta) + \frac{y}{z}\frac{\beta}{\beta_L}\frac{I_{yy}}{I_{zz}}\frac{L}{V}M_L(\theta)}{1 + \frac{y}{z}\frac{\beta}{\beta_L}\frac{I_{yy}}{I_{zz}}\frac{L}{V}} \tag{5}$$

where $1/\beta$ and $1/\beta_L$ are the characteristic vertical and lateral bending wavelengths for the rail on a given foundation (see Appendix A), I_{yy} and I_{zz} are the second area moments of the rail section for vertical and lateral bending, L/V is the ratio of lateral to vertical load, and

$$M_v(\theta) = 1 + \frac{(b/z)\kappa^2 E_I(\kappa)\sin\theta}{(1+\kappa^2)E_I(\kappa) + (1-\kappa^2)E_{II}(\kappa)} \tag{6}$$

and

$$M_L(\theta) = 1 + \frac{(a/y)\kappa^2 E_I(\kappa)\cos\theta}{(1-2\kappa^2)E_I(\kappa) - (1-\kappa^2)E_{II}(\kappa)} \tag{7}$$

where $\kappa^2 = 1 - (b/a)^2$. Also, E_I and E_{II} are the complete elliptic integrals of the first and second kind, respectively, defined by

$$E_I(\kappa) = \int_0^{\pi/2} \sqrt{1-\kappa^2\sin^2\phi}\,d\phi \qquad E_{II}(\kappa) = \int_0^{\pi/2} \frac{d\phi}{\sqrt{1-\kappa^2\sin^2\phi}} \tag{8}$$

Equations (6) and (7) were derived originally by Shah and Kobayashi [14] for elliptic flaws. The dependency of the stress intensity factor on position along the crack front can be eliminated by calculating a simple average value. This concept can be generalized to calculate the $P^{\underline{th}}$ root-mean value where P is the exponent of ΔK in the crack growth rate equation

$$M_G = \frac{\left[\int_0^{\pi/2} M(\theta)^P \rho\,d\theta\right]^{1/P}}{\left[\int_0^{\pi/2} \rho\,d\theta\right]^{1/P}} \tag{9}$$

where

$$\rho = \frac{b}{\sqrt{\sin^2\theta + (b/a)\cos^2\theta}} \tag{10}$$

is the radius of the corner flaw measured from the origin to the perimeter. Equation (9) includes the special case of P = 1, which is the calculation for a simple average.

Table 2 summarizes the stress-gradient magnification factor, as given by equation (9) for the 4th root mean. The table lists the magnification factor as a function of crack size (in terms of percent head area) and lateral-to-vertical load ratio for an unworn or new 132 RE rail section.

Table 2. Stress-Gradient Magnification Factors for Unworn 132 RE Rail Section (P = 4)

RDF Size (% HA)	Lateral-to-Vertical Load Ratio, L/V					
	0.05	**0.10**	**0.20**	**0.30**	**0.40**	**0.50**
10	0.978	0.960	0.934	0.915	0.901	0.891
20	0.969	0.944	0.908	0.882	0.863	0.849
30	0.962	0.932	0.888	0.858	0.836	0.819
40	0.956	0.922	0.872	0.838	0.813	0.795
50	0.951	0.913	0.858	0.821	0.794	0.775
60	0.946	0.905	0.846	0.806	0.778	0.757
70	0.942	0.898	0.834	0.793	0.763	0.742
80	0.938	0.891	0.824	0.781	0.750	0.729

2.3 LIFE CALCULATION

A Paris-Walker type equation [15] was assumed in the crack growth analyses

$$\frac{da}{dN} = C\frac{\Delta K_I^P}{(1-R)^Q} \tag{11}$$

where a is the radius of the defect, N is the number of stress cycles, ΔK is the stress intensity factor range, and R is defined as the ratio between the minimum and maximum stress in a given cycle (called the stress ratio). In this equation, C, P, and Q are empirically determined constants. The following constants were assumed for rail steel: $C = 1 \times 10^{-11}$, $P = 4$, and $Q = 1.63$.

A special provision must be made when applying equation (11) to crack growth calculations involving values of R less than zero. Physically, a negative value of R means that the minimum stress in the given cycle is compressive, and that the opposing crack surfaces are in contact. This phenomenon is known as crack closure. The physical significance of crack closure in fatigue is that crack growth cannot occur while the crack surfaces are in contact. Mathematically, negative values of R are made equivalent to $R = 0$ (no closure) when equation (11) is carried out in the crack growth analyses.[10]

From equation (2), the stress intensity factor range for the RDF defect is defined as

$$\Delta K = \frac{2}{\pi} M_1(a) M_G(a) \Delta\sigma\sqrt{\pi a} \tag{12}$$

where $\Delta\sigma$ is the stress range for a given cycle. When combined with equation (11), the Paris-Walker growth-rate equation can be treated as a separable differential equation in which crack radius (or equivalently, crack size) is the independent variable and cycles is the dependent variable. As such, integration of the crack growth equation results in an expression that separates the geometry effects from the loading effects [17]:

$$n = \frac{\displaystyle\int_{a_1}^{a_2} \frac{da}{\left[\frac{2}{\pi} M_1(a) M_G(a)\sqrt{\pi a}\right]^P}}{C\sum \frac{\Delta\sigma^P}{(1-R)^Q}} = \frac{\text{Geometry Integral}}{\text{Stress Spectrum Sum}} \tag{13}$$

[10] Fatigue experiments have demonstrated that crack closure can occur when R is greater than zero (tension-tension cycling). Crack closure, however, is neglected in the present analyses for RDF defects. Additional discussions on crack closure can be found in Reference [16].

where n is the number of four-axle-load groups to grow a quarter-circular defect of radius a_1 to a quarter-circular defect of radius a_2 with the same aspect ratio.[11] The summation is performed over the five stress cycles in the simplified stress spectrum produced from the four-axle loads in the coupled hopper car configuration (recall Section 2.1.1). In the crack growth calculations, the number of four-axle-load groups is converted to an equivalent measure of accumulated tonnage in terms of million gross tons (MGT) of traffic.

2.4 ANALYSIS FOR WORN RAIL

The cross-section of an actual rail can be approximated by an idealized section consisting of three rectangular areas representing the head, web, and base of the rail (Figure 5). Wear of the rail is approximated by loss of material or a change in area of the rectangle representing the head only. In the present analysis, wear is quantified by a percentage of the rail head area.

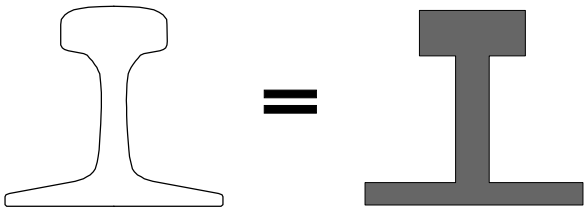

Figure 5. Actual and Idealized Rail Cross-Sections

Equivalence between the actual and idealized rails is achieved by matching section properties for both cross-sections. The second area moments of inertia for the rail head about the vertical and horizontal axes through the centroid are related to the rectangular cross-section by

$$I_{zz_H} = \frac{1}{12} h_{eq} w_{eq}^3 \qquad I_{yy_H} = \frac{1}{12} h_{eq}^3 w_{eq} \tag{14}$$

These equations can be rearranged so that w_{eq} is on the left-hand side

$$w_{eq}^3 = \frac{12 I_{zzH}}{h_{eq}} \qquad w_{eq} = \frac{12 I_{yyH}}{h_{eq}^3} \tag{15}$$

The equivalent rail-head height can be found by combining these two equations to eliminate w_{eq}

[11] The present analysis neglects the effect of load sequence on the fatigue life. This effect is discussed in Reference [18].

$$w_{eq}^3 = \frac{12 I_{zz_H}}{h_{eq}} = \frac{12^3 I_{yy_H}^3}{h_{eq}^9} \tag{16}$$

from which

$$h_{eq} = \sqrt[8]{144 \frac{I_{yyH}^3}{I_{zzH}}} \tag{17}$$

An expression for the equivalent rail-head width can be found through similar algebraic manipulations

$$w_{eq} = \sqrt[8]{144 \frac{I_{zzH}^3}{I_{yyH}}} \tag{18}$$

For a 132 RE rail section, h_{eq} = 1.528 inches and w_{eq} = 2.815 inches. The cross-sectional area of the idealized rail head is the product of the equivalent height and width, or 4.30 in^2. This value is 2.6% lower than the actual rail-head area of 4.42 in^2, which is within reasonable engineering approximation.

In the present analysis, loss of material from wear is modeled geometrically in two ways; either uniform loss of rail-head height off the top of the rail or uniform loss of head width off the gauge side. These two idealized patterns for rail-head wear are shown schematically in Figure 6.

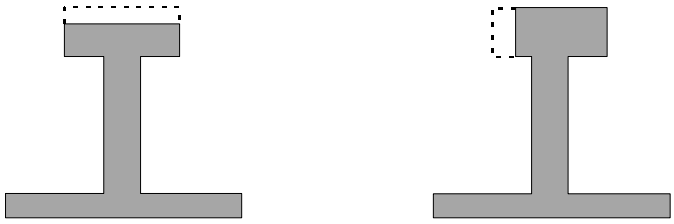

(a) Loss of Rail Head Height **(b) Loss of Rail Head Width**

Figure 6. Idealized Rail-Head Wear Patterns

In the crack propagation analyses for worn rail, a percentage of the rail-head area is removed by decreasing the equivalent rail-head height or width by the same percentage. The section properties required for the rail bending stress analysis are estimated from the idealized cross-section with a decreased rail head area. The rail section properties affected by wear include

I_{yyH} = area moment of inertia for vertical bending of the rail head only
I_{zzH} = area moment of inertia for horizontal bending of the rail head only
I_{yy} = area moment of inertia for vertical bending of the entire rail
I_{zz} = area moment of inertia for horizontal bending of the entire rail
C = torsion constant of the entire rail
D = warping constant of the entire rail
z_H = distance from the bottom of the rail to the centroid of the rail head only
z_N = distance from the bottom of the rail to the centroid of the entire rail
z_C = distance from the bottom of the rail to the shear center

The methodologies developed to determine the section properties for rails with the two assumed wear patterns are described in the next two subsections.

2.4.1 Loss of Rail-Head Height

Wear can be assumed to occur from uniform loss of material across the top of the rail head. In this case, the second area moment of inertia about the rail-center plane for the entire rail can be calculated by simply adding the lateral bending inertia for the head, web, and base

$$I_{zz_{RAIL}} = I_{zz_H} + I_{zz_W} + I_{zz_B} \tag{19}$$

The parallel-axis theorem, however, must be applied to determine the vertical bending inertia because the neutral axis of the entire rail shifts from the loss of material. This concept is shown schematically in Figure 7.

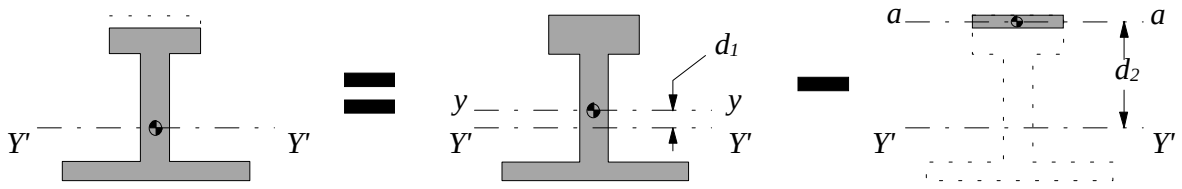

Figure 7. Schematic for Vertical Bending Inertia Calculation for Rail-Head Height Loss

Referring to this figure, the second area moment of inertia about the horizontal axis through the centroid of a rail with head-height loss is equal to

$$I_{Y'Y'} = \left[I_{yy} + A_R d_1^2\right] - \left[I_{aa} + A_{aa} d_2^2\right] \tag{20}$$

where I_{yy} is the vertical bending inertia for the unworn or new rail, A_R is the cross-sectional area of the new or unworn rail, d_1 is the distance between the centroids

of the worn and unworn rails, I_{aa} is the vertical bending inertia for the worn area, A_{aa} is the amount of worn area, and d_2 is the distance between the centroid of the entire worn rail to the centroid of the worn-away area.

In addition to the vertical and lateral bending inertias, other rail section properties, which are required in the rail stress analysis, are affected by wear. These section properties include the location of the centroid for the rail and for the rail head only, location of the shear center, and polar moments of inertia. The equations to determine section properties for worn rail in terms of head-height loss are listed in Appendix B. Table 3 lists estimated values of section parameters for 132 RE rail with various levels of wear in terms of percentage of head area.

Table 3. Estimated Section Properties for 132 RE Rail with Loss of Head Height

Wear (% HA)	I_{yyH} (in^4)	I_{zzH} (in^4)	I_{yy} (in^4)	I_{zz} (in^4)	$C\times10^7$ ($lb\text{-}in^2$)	$D\times10^7$ ($lb\text{-}in^2$)	z_H (in)	z_N (in)	z_C (in)
0	0.84	2.84	88.2	14.2	6.04	6.78	6.30	3.20	1.63
10	0.61	2.56	84.7	13.9	5.46	6.23	6.22	3.09	1.52
20	0.43	2.27	81.5	13.6	4.91	5.66	6.15	2.97	1.41
30	0.29	1.99	78.5	13.3	4.40	5.06	6.07	2.84	1.29
40	0.18	1.70	75.8	13.1	3.92	4.43	5.99	2.71	1.18
50	0.11	1.42	73.4	12.8	3.48	3.78	5.92	2.56	1.06

Since wear affects the geometry of the rail head, the finite section magnification factor in the stress intensity factor formula should be adjusted to account for the loss of material due to wear. Table 4 lists the finite section magnification factors for various defect sizes and rail sections for reduced head area. Similarly, the stress-gradient magnification factor is also affected by the reduction in head area. Recall that equation (5) depends on the second area moments of inertia for vertical and lateral bending, which change with the level of wear. Table 5 lists the corresponding stress-gradient magnification factors for 132 RE rail with two levels of head-height loss.

Table 4. Finite-Section Magnification Factors for Worn Rail

(a) Worn area = 20% HA

RDF Size (% HA)	Rail Size					
	70 ASCE	100 RE	115 RE	132 RE	136 RE	140 RE
10	1.227	1.225	1.223	1.223	1.224	1.224
20	1.281	1.274	1.267	1.266	1.271	1.270
30	1.362	1.348	1.333	1.330	1.340	1.339
40	1.472	1.448	1.421	1.416	1.434	1.433
50	1.616	1.577	1.535	1.527	1.555	1.553
60	1.799	1.741	1.677	1.666	1.708	1.705
70	2.030	1.946	1.853	1.837	1.897	1.893
80	2.323	2.201	2.069	2.047	2.132	2.126

(b) Worn area = 40% HA

RDF Size (% HA)	Rail Size					
	70 ASCE	100 RE	115 RE	132 RE	136 RE	140 RE
10	1.235	1.232	1.229	1.228	1.231	1.230
20	1.308	1.297	1.286	1.284	1.292	1.291
30	1.419	1.397	1.373	1.369	1.385	1.383
40	1.575	1.536	1.492	1.485	1.513	1.511
50	1.785	1.719	1.648	1.636	1.682	1.679
60	2.061	1.958	1.848	1.830	1.901	1.895
70	2.426	2.268	2.104	2.077	2.181	2.173
80	2.917	2.675	2.430	2.391	2.545	2.533

Table 5. Stress-Gradient Magnification Factors for 132 RE Rail Section with Loss of Head Height (P = 4)

(a) Worn area = 20% HA

RDF Size (% HA)	Lateral-to-Vertical Load Ratio, L/V					
	0.05	**0.10**	**0.20**	**0.30**	**0.40**	**0.50**
10	0.981	0.966	0.942	0.924	0.910	0.900
20	0.974	0.952	0.919	0.894	0.876	0.861
30	0.968	0.941	0.901	0.872	0.850	0.833
40	0.963	0.933	0.887	0.854	0.829	0.810
50	0.959	0.925	0.874	0.838	0.812	0.791
60	0.955	0.918	0.863	0.824	0.796	0.775
70	0.951	0.912	0.853	0.812	0.782	0.760
80	0.948	0.906	0.844	0.801	0.770	0.747

(b) Worn area = 40% HA

RDF Size (% HA)	Lateral-to-Vertical Load Ratio, L/V					
	0.05	**0.10**	**0.20**	**0.30**	**0.40**	**0.50**
10	0.985	0.971	0.950	0.933	0.920	0.910
20	0.978	0.960	0.930	0.907	0.889	0.875
30	0.973	0.951	0.915	0.887	0.866	0.849
40	0.969	0.943	0.902	0.871	0.847	0.828
50	0.966	0.937	0.891	0.857	0.831	0.810
60	0.962	0.931	0.881	0.845	0.816	0.794
70	0.959	0.925	0.872	0.833	0.804	0.781
80	0.957	0.921	0.864	0.823	0.792	0.768

2.4.2 Loss of Rail-Head Width

A second wear pattern was assumed where material was lost uniformly from the gauge-side face of the rail head. In this wear configuration, the locations of the rail centroid and the shear center shift from the plane of the vertical centerline. Therefore, in the case of gauge-side wear, the parallel-axis theorem must be applied to determine the second area moments of inertia for both vertical and lateral bending. In the previous case of wear from head-height loss, the centroid and center of twist of the worn rail were located along the vertical centerline because the rail cross-section remained symmetric about that plane after wear. Figure 8 is a schematic illustration of the application of the parallel-axis theorem for the calculation of the second area moment for lateral bending.

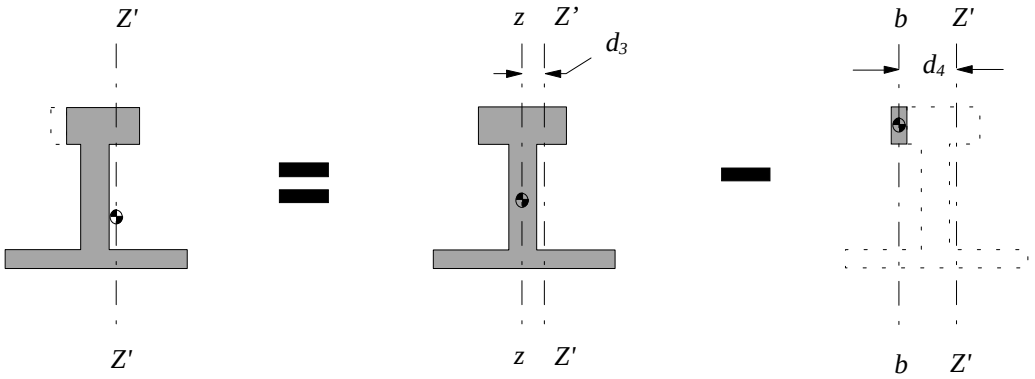

Figure 8. Schematic of Lateral Bending Inertia Calculation for Rail with Head-Width Loss

Referring to the figure and according to the parallel-axis theorem, the lateral bending inertia for a worn rail is equal to the lateral bending inertia with respect to the centroid of the worn rail minus the lateral bending inertia of the worn area

$$I_{Z'Z'} = \left[I_{zz} + A_R d_3^2\right] - \left[I_{bb} + A_{bb} d_4^2\right] \tag{21}$$

where I_{zz} is the lateral bending inertia for the unworn or new rail, d_3 is the horizontal distance between the centroids of the worn and unworn rails, I_{bb} is the lateral bending inertia of the worn area, A_{bb} is the amount of worn area, and d_4 is the distance between the centroid of the worn rail and the centroid of the worn area. Correspondingly, the second area moment of inertia for vertical bending is calculated in a similar manner, as shown in Figure 9.

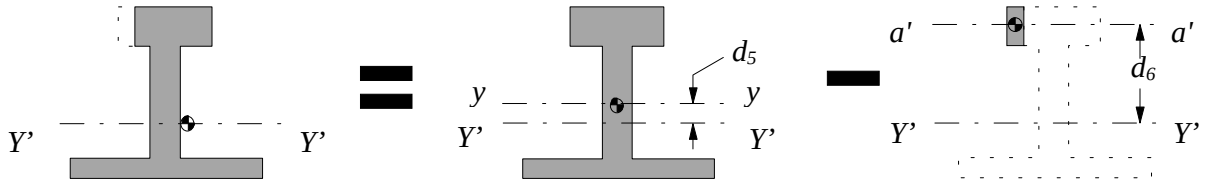

Figure 9. Schematic of Vertical Bending Inertia Calculation for Rail with Head-Width Loss

Thus, the vertical bending inertia for the entire rail with a reduced head width can be determined from

$$I_{Y'Y'} = \left[I_{yy} + A_R d_5^2\right] - \left[I_{a'a'} + A_{a'a'} d_6^2\right] \tag{22}$$

where d_5 is the distance between the centroids of the worn and unworn rails, $I_{B'B'}$ is the vertical bending inertia for the worn area, $A_{B'B'}$ is the area of worn material from the gauge-side face, and d_6 is the distance between the centroids of the worn rail and the worn area.

The equations used in the model to determine section properties of worn rail with a reduced head width are included in Appendix B. Table 6 lists the section properties for various levels of wear as estimated by these equations. This table includes three more additional section properties than were listed in the corresponding table for head-height loss, namely:

y_H = distance from the vertical centerline to the centroid of the rail head only
y_N = distance from the vertical centerline to the centroid of the entire rail
y_C = distance from the vertical centerline to the shear center

Table 6. Estimated Section Properties for 132 RE Rail with Loss of Rail-Head Width

Wear (% HA)	I_{yyH} (in^4)	I_{zzH} (in^4)	I_{yy} (in^4)	I_{zz} (in^4)	$C\times10^7$ (lb-in^2)	$D\times10^7$ (lb-in^2)	y_H (in)	y_N (in)	z_N (in)	y_C (in)	z_C (in)
0	0.84	2.84	88.2	14.2	6.04	6.78	0	0	3.20	0	1.63
10	0.75	2.07	83.7	13.5	5.24	5.24	0.14	0.05	3.09	0.09	1.36
20	0.67	1.45	78.9	13.0	4.58	3.86	0.28	0.08	2.97	0.18	1.12
30	0.59	0.97	73.7	12.7	4.04	2.69	0.42	0.11	2.85	0.26	0.91
40	0.50	0.61	68.1	12.6	3.63	1.74	0.56	0.13	2.71	0.32	0.74
50	0.42	0.36	62.1	12.5	3.31	1.03	0.70	0.15	2.56	0.37	0.62

As in the case of head-height loss, wear in terms of reduced rail-head width also affects the finite-section and stress-gradient magnification factors that are used to calculate the stress intensity factor for RDF defects. The finite-section correction for rails with reduced head-width are the same as for those with equivalent wear in percent head area for head-height loss, as listed in Table 4, because the equation for finite boundaries depends only on the cross-sectional areas of the rail and the rail head and not on the wear pattern (i.e., wear from head-height loss or reduced head width). The stress-gradient magnification, however, is affected by the wear pattern because loss of material from the gauge-side face influences the bending inertias needed to calculate the stress-gradient correction, as given by equations (5) through (10) . Table 7 lists the stress-gradient magnification factors for 132 RE rail and two levels of wear in terms of material loss from the gauge-side face.

Table 7. Stress-Gradient Magnification Factors for 132 RE Rail Section with Loss of Head Width (P = 4)

(a) Worn area = 20% HA

RDF Size (% HA)	Lateral-to-Vertical Load Ratio, L/V					
	0.05	**0.10**	**0.20**	**0.30**	**0.40**	**0.50**
10	0.979	0.961	0.932	0.908	0.889	0.873
20	0.971	0.946	0.904	0.872	0.847	0.826
30	0.964	0.934	0.884	0.846	0.816	0.792
40	0.959	0.924	0.867	0.825	0.792	0.766
50	0.954	0.915	0.853	0.807	0.771	0.744
60	0.950	0.907	0.840	0.791	0.754	0.726
70	0.946	0.900	0.829	0.777	0.739	0.710
80	0.942	0.894	0.819	0.765	0.725	0.697

(b) Worn area = 40% HA

RDF Size (% HA)	Lateral-to-Vertical Load Ratio, L/V					
	0.05	**0.10**	**0.20**	**0.30**	**0.40**	**0.50**
10	0.982	0.965	0.934	0.906	0.880	0.858
20	0.975	0.951	0.907	0.869	0.835	0.806
30	0.969	0.940	0.888	0.842	0.803	0.770
40	0.964	0.931	0.872	0.821	0.778	0.742
50	0.960	0.923	0.858	0.802	0.757	0.719
60	0.956	0.916	0.845	0.786	0.739	0.701
70	0.953	0.910	0.834	0.772	0.723	0.685
80	0.950	0.904	0.824	0.760	0.710	0.672

3. SENSITIVITY STUDIES

The RDF model was used to analyze several hypothetical cases, in order to gain some insight into the sensitivity of RDF safe crack-growth life to service conditions. The sensitivity studies were performed by establishing a set of baseline service conditions. Each condition was varied at a single time while holding the other parameters at their baseline values. Table 8 lists the assumed baseline parameters used in the sensitivity studies for RDF defects. The baseline also included residual stress levels reflecting those typically found in measurements of rail samples taken from both tangent and curved track. The residual stress function shown in Figure 3 was used in these studies with a severity level or magnification factor equal to 1.0. The effects of residual stress are examined by varying the severity level from this baseline value.

Table 8. Baseline Parameters for Sensitivity Studies

Parameter	Value
Foundation stiffness	2,000 psi
Track curvature	5-degree curve
Rail size	132 RE
Dynamic load factor	1.3
Rail wear	None
Service temperature	No thermal tension
Residual stress severity level	1.0

The results of the sensitivity studies are presented in terms of safe crack-growth life expressed in million gross tons (MGT) and "critical" crack or defect sizes expressed as percentages of rail-head area (% HA). The crack growth life is the number of four-axle load groups, converted to MGT, predicted for RDF defect growth from a detectable size to the "critical" crack size. A detectable RDF size[12] of 10% HA was assumed for the purpose of these studies. "Critical" crack size is the predicted RDF size at which a rail of average fracture toughness (35 ksi-in$^{1/2}$) is expected to fail from the maximum stress produced by the simplified four-axle load group.[13]

3.1 EFFECT OF WEAR

The propagation analyses of RDF defects in worn rails assumed that the amount of wear was constant throughout the life of the defect. In other words, the model assumes that the entire wear of the rail occurs prior to defect formation, and that no further wear occurs while the RDF defect propagates to critical size.

[12] Experience with rail test equipment must be relied upon to estimate the "detectable" size for use in the model. A common practice is to choose a size for which field experience suggests roughly one out of three similar defects is detected.

[13] The model predicts critical RDF sizes up to 80% HA.

Figure 10 compares the effect of wear pattern on the RDF growth rate. This result indicates that a rail with head-height loss has a shorter fatigue life than one with an equivalent reduction in cross-sectional area from the gauge-face side. For the two wear patterns shown in Figure 10, the rail-head cross-sectional area has been reduced by 40%. Moreover, head-height loss gives more conservative estimates for safe crack-growth life and critical crack size than gauge-face side wear. A comparison of the section properties listed in Tables 3 and 6 reveals that the vertical bending inertia for the rail head only (I_{yyH}) correlates with this result. Unless it is stated otherwise, wear should be interpreted as head-height loss in the remainder of this report.

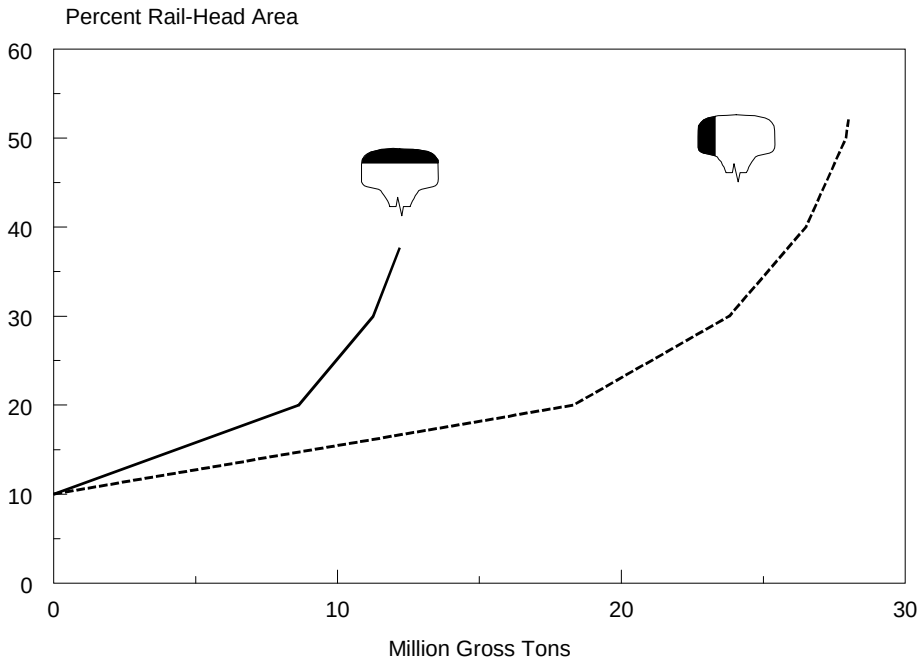

Figure 10. Effect of Wear Pattern on RDF Growth

Figure 11 shows the safe crack-growth life for three levels of rail-head wear (i.e., head-height loss) in terms of percentage of head area. The effect of head-height loss on the critical RDF size is shown in Figure 12. A 20% loss in head height reduces the RDF safe crack-growth life by over 40% from the baseline value (no wear); a 40% loss reduces RDF safe life by more than 70%. The critical size for 20% loss in head height is about 25% smaller than the baseline value; for a 40% loss, the critical crack size is about half of the baseline. Both figures also show the results of regression analyses performed to determine the “best-fit” curve by means of the calculated values.

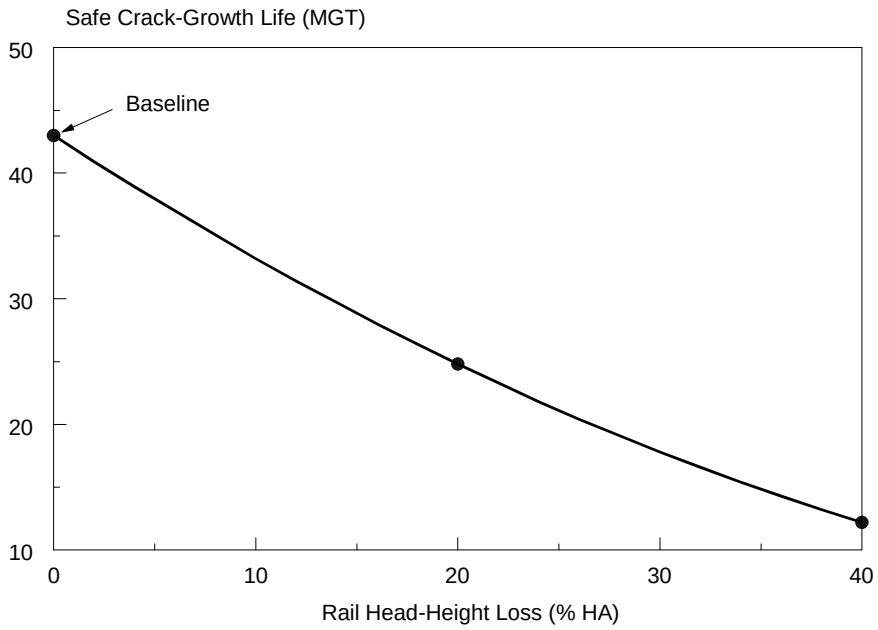

Figure 11. Effect of Head-Height Loss on RDF Safe Crack-Growth Life

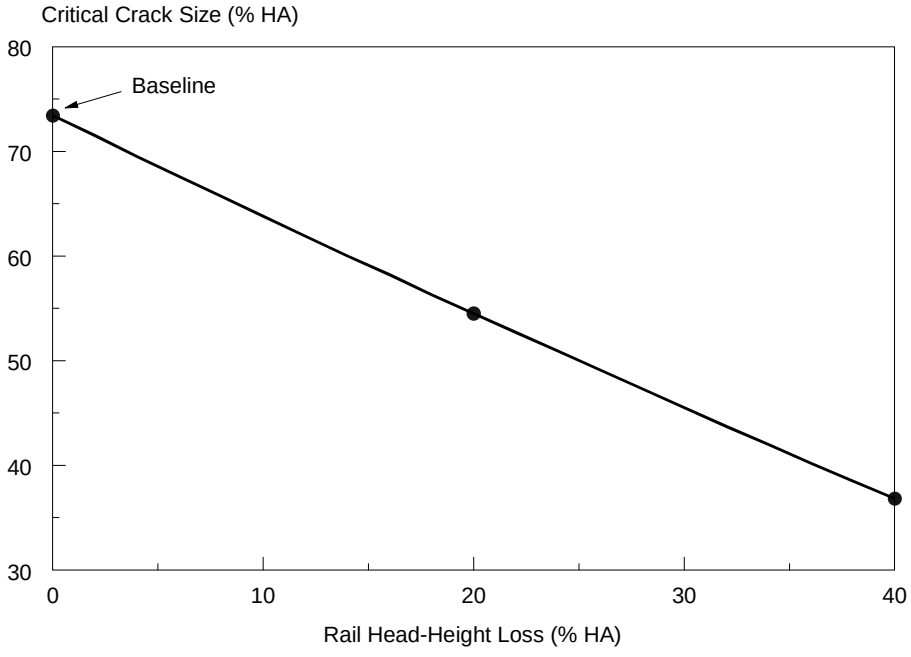

Figure 12. Effect of Head-Height Loss on Critical RDF Size

The relation between safe crack-growth life and head-height loss is clearly nonlinear, as shown in Figure 11. But, as shown in Figure 12, the critical RDF defect size is practically a linear function of head-height loss.

3.2 EFFECT OF THERMAL STRESS

The effect of the thermal stress history on the RDF defect growth behavior can be included in the present analysis if the relation between thermal stress and either defect size or tonnage (MGT) is known *a priori*.

In the sensitivity studies presented here, however, thermal stresses were examined by assuming an average or constant difference between the service temperature and the neutral or stress-free temperature. This simplifying assumption is essentially equivalent to an uniform, tensile residual stress field in the rail. In addition to the baseline case (no thermal tension), three values of constant temperature difference were assumed in the sensitivity studies. Table 9 lists the magnitudes of the thermal stresses associated with these temperature differences, according to equation (1) in Section 2.1.3. Temperature differences of 25°F can be easily exceeded during the winter months in North America.

Table 9. Tensile Thermal Stress for Various Temperature Differences

ΔT (°F)	Constant Thermal Stress (ksi)
5	0.975
10	1.950
25	4.875

Figure 13 shows the safe crack-growth life of RDF defects for four levels of thermal tension. Thermal tension equal to 1 ksi reduces the safe life by about 25% from the baseline value; thermal tension of about 5 ksi reduces it by more than 75% from the baseline. Thus, the relation between safe crack-growth life and temperature difference or equivalently thermal tension is nonlinear. The figure also shows a “best-fit” regression curve, which can be used to interpolate the safe life for intermediate temperature differences.

The effect of thermal tension on the critical size of RDF defects is shown in Figure 14. The regression curve in this plot suggests that the relation between thermal tension in terms of temperature difference and critical crack size is roughly linear. Thermal tension corresponding to ΔT = 25°F reduces the critical RDF size by about 45% from the baseline case.

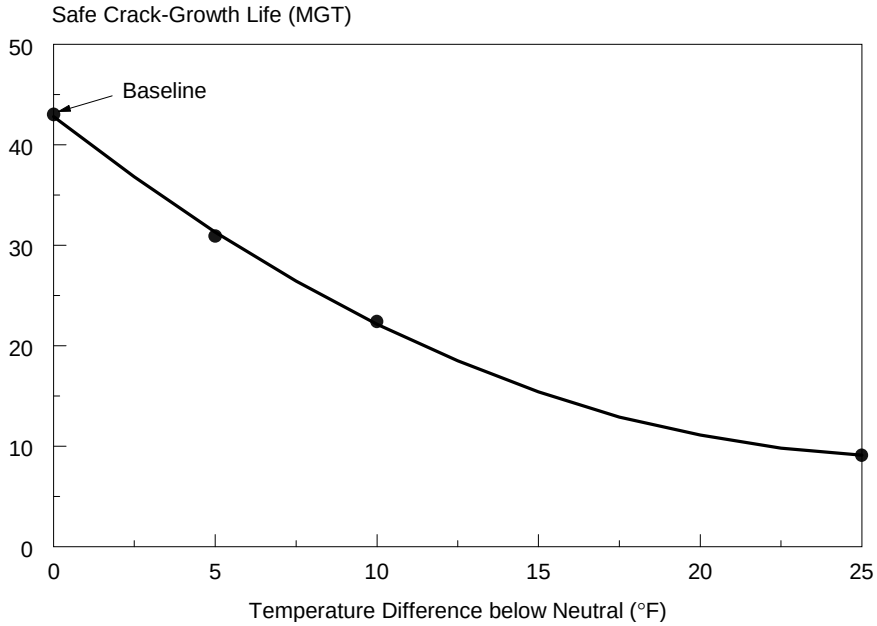

Figure 13. Effect of Thermal Tension on RDF Safe Crack-Growth Life

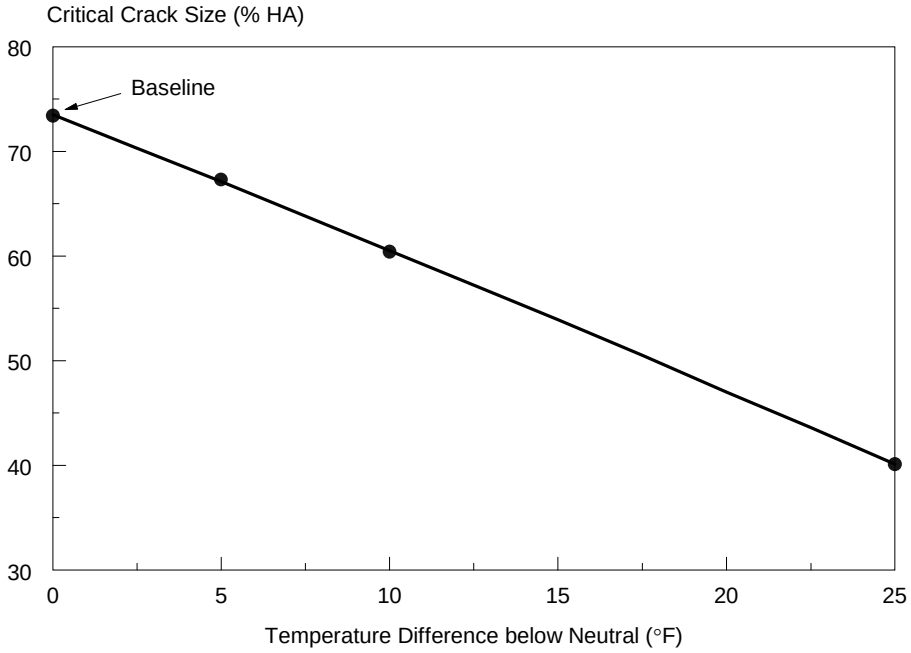

Figure 14. Effect of Thermal Tension on Critical RDF Size

3.3 EFFECT OF RESIDUAL STRESS

The relation of residual stress and flaw size, as shown previously in Figure 3, was determined from strain measurements on a rail section taken from curved track (see Section 2.1.2). The effect of residual stress was examined through varying the magnitude of the residual stresses in Figure 3 by applying a multiplying factor, which was assumed to assess the severity level. The severity factor could refer to the rail quality; for example, rail steel with a lower yield strength could have higher residual stresses. Severity could also refer to previous tonnage; heavier traffic could also increase residual stress levels.

In addition to the baseline (severity factor or SF = 1.0), two other levels of severity were assumed in the sensitivity studies. Figure 15 indicates that the residual stress severity level has a significant effect on the safe crack-growth life of RDF defects. The range of safe crack-growth lives varies between 2.1 MGT (for SF = 3.0) and 43.0 MGT corresponding to the baseline (SL = 1.0). The safe life decreases by slightly more than 80% when the severity factor is doubled from the baseline; and by about 95% when the severity factor is tripled. Clearly, the relation between safe crack-growth life and the residual-stress severity factor is nonlinear.

Figure 16 shows that the relation between critical RDF size and the residual-stress severity factor is also nonlinear. The range of critical RDF defects sizes varies between 20.5% HA (corresponding to SL = 3.0) and 73.4% HA for the baseline case.

3.4 EFFECT OF RAIL SIZE

For the sake of convenience, rail size is often characterized by weight per yard. For the purpose of sensitivity studies, however, a more appropriate descriptor for rail size is the second area moment of inertia with respect to the horizontal axis through the centroid (I_{yy}) because of its relatively large influence on the magnitude of the vertical bending stress.

Figure 17 shows the effect of the vertical bending inertia on the safe crack-growth life of RDF defects. A wide variety of rail sizes is shown on the plot, ranging from a very light rail (70 ASCE) to a somewhat heavy rail section (155 PS). The results of a regression analysis, indicated by the solid line on the plot, suggest that the safe crack-growth life is a linear function of the second area moment of inertia for vertical bending.

An apparent linear relation between the critical RDF defect size and the vertical bending inertia is shown in Figure 18. The critical defect size varies between 42.8% HA for 70 ASCE to greater than 80% HA for 155 PS.

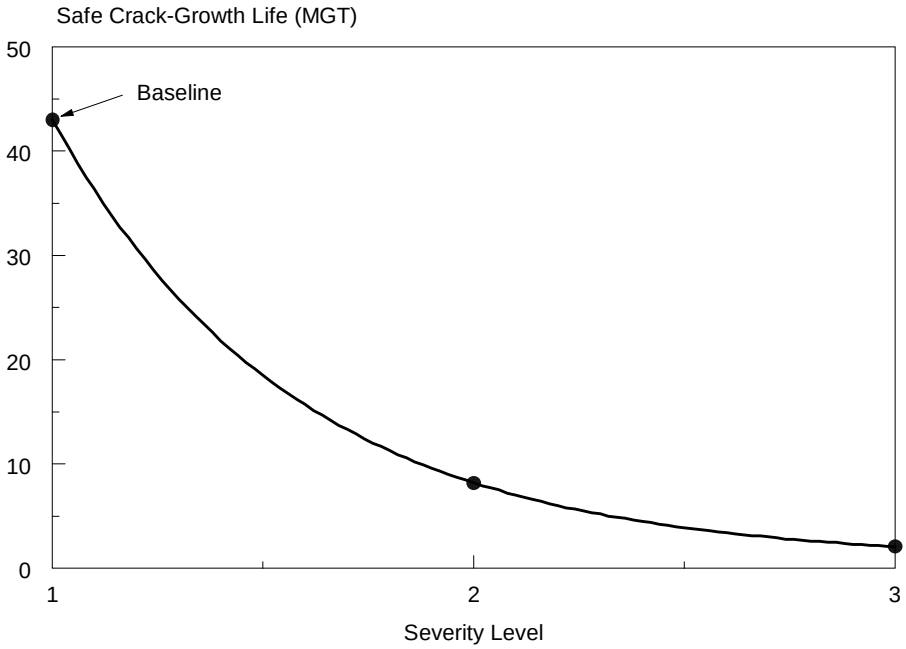

Figure 15. Effect of Residual Stress Severity Level on RDF Safe Crack-Growth Life

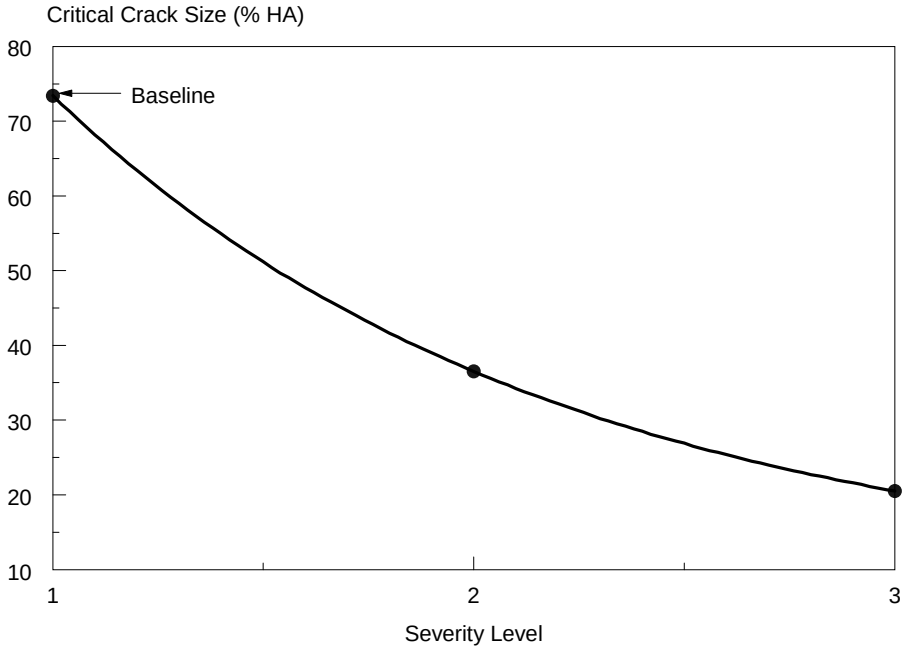

Figure 16. Effect of Residual Stress Severity Level on Critical RDF Size

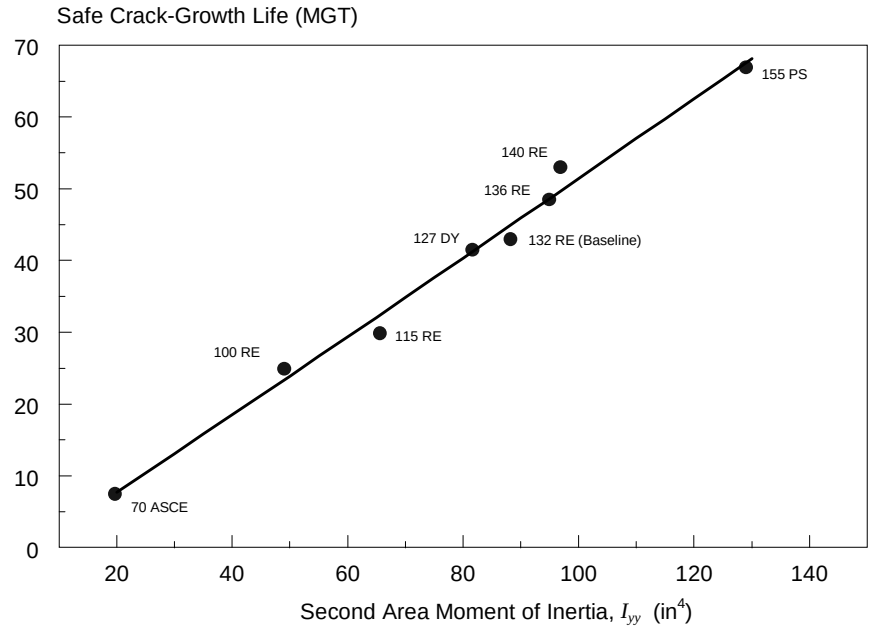

Figure 17. Effect of Rail Size on RDF Safe Crack-Growth Life

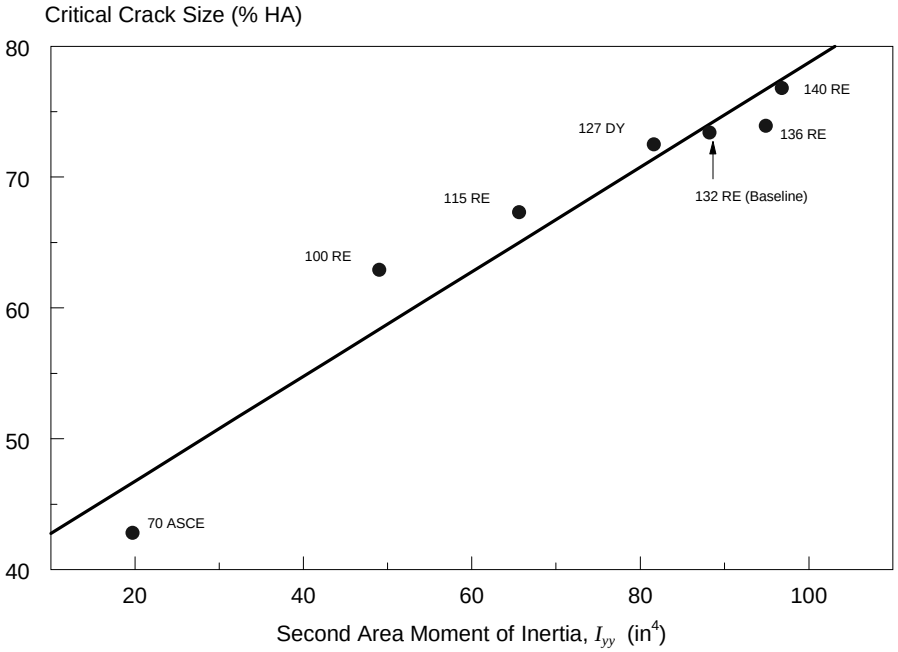

Figure 18. Effect of Rail Size on Critical RDF Size

3.5 EFFECT OF TRACK CURVATURE

In the RDF defect growth model, variations in track curvature refer to changes in the wheel/rail loading characteristics. In particular, the ratio of lateral-to-vertical wheel load and the location of wheel/rail contact with respect to vertical centerline depend on track curvature. Table 10 lists the loading characteristics corresponding to various track curvatures, as assumed in the sensitivity studies presented here.

Table 10. Load Descriptions for Varying Track Curvature

Track Curvature	*L/V* Ratio	Vertical Load Offset
Tangent	0.05	0.25 head width
5-degree ("mild") curve	0.30	0.50 head width
8-degree ("sharp") curve	0.40	0.50 head width

Figure 19 illustrates the relation between safe crack-growth life and track curvature. The figure shows that the safe crack-growth life of an RDF defect in an 8-degree curve is reduced by about 35% from the baseline (i.e., 5-degree curved track). Conversely, the safe life of an RDF defect in tangent track is increased by more than 140% over the baseline.

Figure 20 shows the relation between critical RDF defect size and track curvature. The dashed line on the plot represents an extrapolation because the analysis did not predict a precise value for the critical size of an RDF defect in tangent track. For the tangent track case, the analysis could only predict that the critical size was greater than 80% HA. The figure does show, however, that the critical RDF defect size in an 8-degree curve is reduced by slightly more than 10% from the baseline.

3.6 EFFECT OF DYNAMIC LOAD FACTOR

Dynamic motions of the carbody and the trucks (pitch, bounce, and rocking) cause variations in the magnitudes of the wheel loads on the rail as trains travel over the track. The American Railroad Engineering Association (AREA) has recommended a simple but convenient formula to account for dynamic motions by magnifying the static wheel load by a factor depending on train speed [19]:

$$DLF = 1 + \frac{33v}{100D} \tag{23}$$

where v is the train speed (in miles per hour) and D is the wheel diameter (in inches).

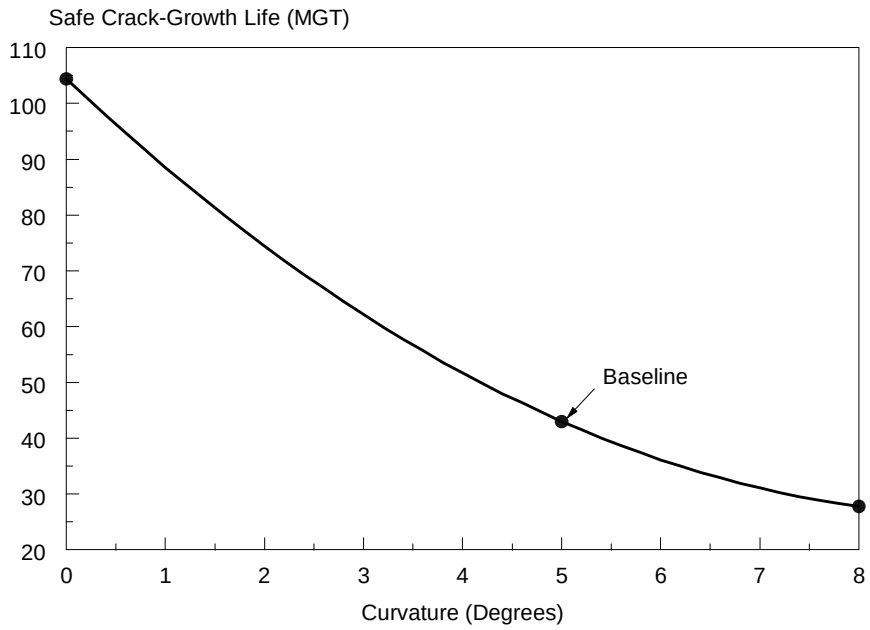

Figure 19. Effect of Track Curvature on RDF Safe Crack-Growth Life

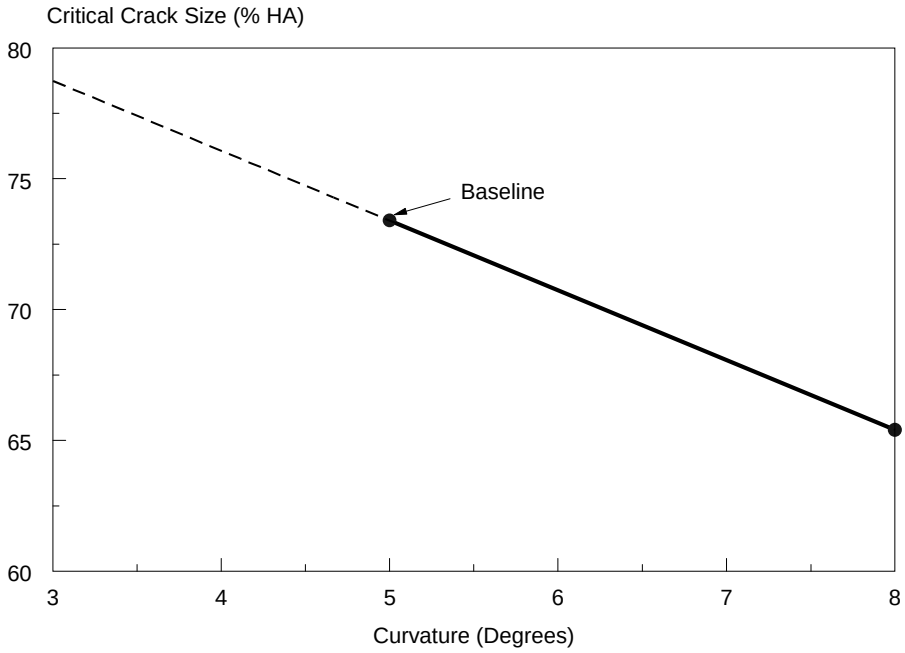

Figure 20. Effect of Track Curvature on Critical RDF Size

According to equation (23), a dynamic load factor of 1.3 corresponds to train speeds between 25 and 33 mph for wheel diameters ranging between 28 and 36 inches. Another formula for dynamic load factor has been adopted by the Indian Railways [20]

$$DLF = 1 + \frac{v}{3\sqrt{k_v}} \tag{24}$$

where v is the train speed (in miles per hour) and k_v is the foundation stiffness (in psi). According to this equation, a dynamic load factor of 1.3 with the baseline value of 2,000 psi for foundation stiffness corresponds to a train speed of slightly more than 40 mph. In both equations, a dynamic load factor of 1.6 corresponds to train speeds that are twice those corresponding to the 1.3 factor.

Figure 21 shows the effect of the dynamic load factor on safe crack-growth life of RDF defects. A dynamic load factor of 1.6 has a safe life that is about 25% less than the baseline value (dynamic load factor of 1.3).

Figure 22 shows the relation between critical RDF size and dynamic load factor. The dashed line in the plot represents an extrapolation because the result corresponding to a dynamic load factor of 1.0 is not a precise number. (In this particular case, the analysis could only predict a critical size greater than 80% HA.) Nevertheless, increasing the dynamic load factor from 1.3 to 1.6 decreases the critical RDF size by about 16%.

3.7 EFFECT OF FOUNDATION STIFFNESS

Four values of foundation stiffness were assumed in the sensitivity studies. The physical interpretation of these values is summarized in Table 11.

Table 11. Representative Vertical Foundation Moduli

k_v (ksi)	Track Description
1 to 2	Poor subgrade; deteriorated ballast; deteriorated wood ties; poorly drained; low-tonnage; low-speed branch line.
2 to 3	Typical mainline freight track; well-maintained ballast and wood ties; 20 to 40 mph operations; 10 to 20 MGT per year.
3 to 5	Well-maintained high-speed, high-tonnage mainline track; ballast and wood ties in excellent condition; 45 to 80 mph operations; 30 to 120 MGT per year. Wood-tie sections of FAST test track.
10	Northeast Corridor concrete-tie track; freight operations up to 60 mph; passenger operations up to 125 mph. Concrete-tie sections of FAST test track.

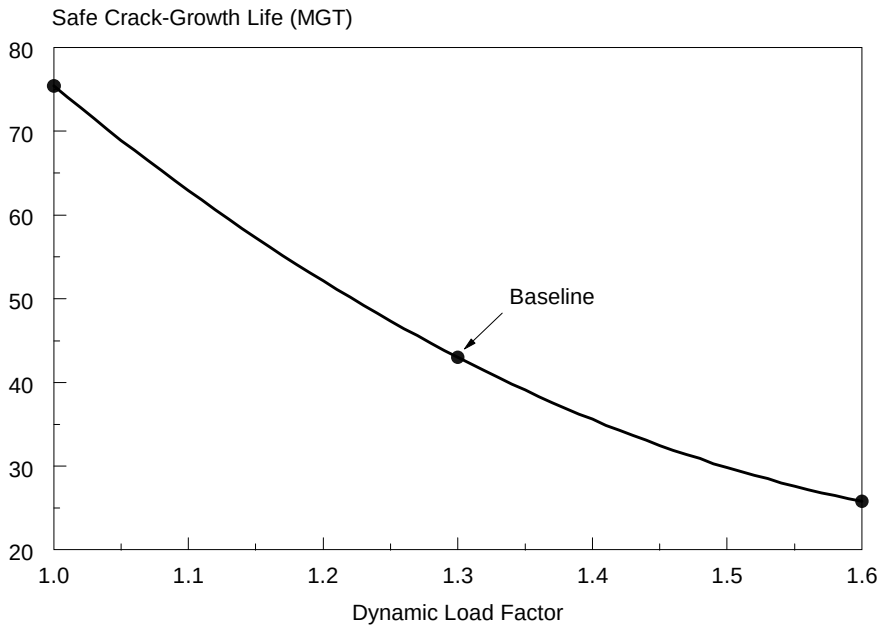

Figure 21. Effect of Dynamic Load Factor on RDF Safe Crack-Growth Life

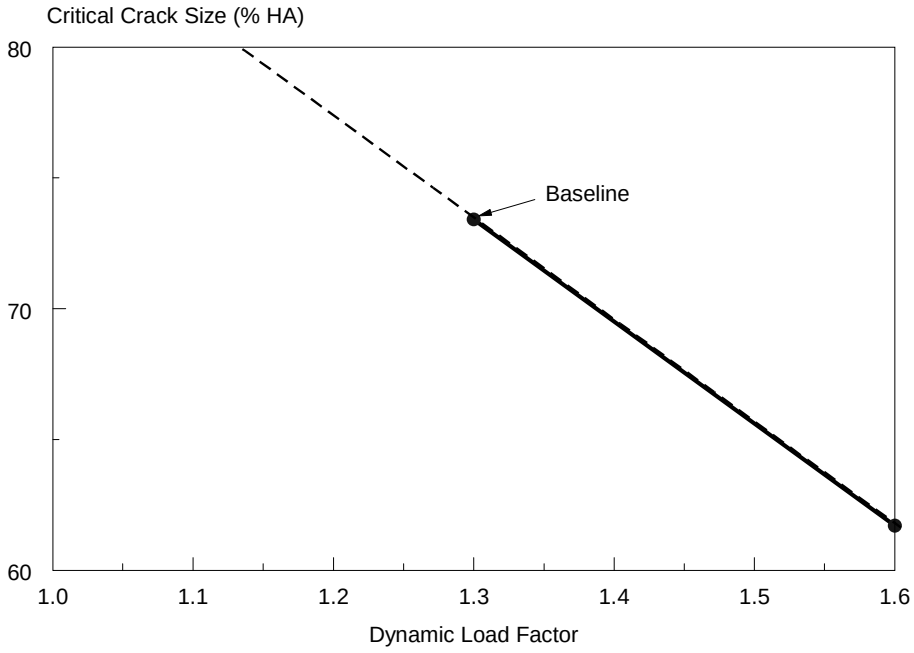

Figure 22. Effect of Dynamic Load Factor on Critical RDF Size

Figure 23 shows the effect of foundation stiffness on RDF safe crack-growth life. Improving the foundation stiffness from 1 to 3 ksi increases the safe crack-growth life by less than 7 MGT, or about 17%. A foundation stiffness of 10 ksi increases the safe life by almost 40% from the baseline.

Figure 24 shows the relation of foundation stiffness and critical RDF defect size. In this plot, the maximum foundation stiffness is 3 ksi because critical RDF sizes were found to be greater than 80% HA for stiffnesses greater than this value. For a foundation stiffness of 1 ksi, the critical defect size is 72.8% HA, which is less than 1% lower than the baseline value.

3.8 SUMMARY OF SENSITIVITY STUDIES

The results of the RDF sensitivity studies are summarized in Figures 25 and 26. Figure 25 shows the trend of each parameter to change the safe crack-growth life relative to the baseline value of 43 MGT. The parameters are arranged in descending order to illustrate the gradation of decrease from the baseline. A similar comparison for the "critical" RDF size, relative to the baseline value of 73.4% HA, is shown in Figure 26. Both figures include the value of the parameter corresponding to the minima and maxima for life and critical size. For example, rail sizes were varied between 70 ASCE and 155 PS, which correspond to safe crack-growth lives ranging from 7.5 to 66.9 MGT, and critical defect sizes between 42.8% HA and greater than 80% HA. In Figure 26, "critical" sizes were predicted to be greater than 80% HA for the cases corresponding to 155 PS rail section, dynamic load factor of 1.0, tangent track loading, and foundation stiffness of 10 ksi (as indicated by the extended bars in the figure for these cases).

Residual stress, rail section, thermal tension, and rail wear have the strongest effects on reducing RDF safe crack-growth life. These factors also have the greatest influence on reducing the critical RDF size, but the relative ranking of these factors is different. The sensitivity studies also show that track curvature has the most significant effect on the range of safe crack-growth life. This result is illustrated by the length of the bar in Figure 25, which represents the range of possible lives for the track curvatures considered in the sensitivity studies. The safe life of RDF defects in an 8-degree curved track is 27.8 MGT compared to 104.4 MGT for an RDF defect in tangent track. Likewise, residual stress is the most influential single factor affecting critical RDF size. The critical sizes vary between 20.5% HA for the most severe residual stress levels and 73.4% HA, which corresponds to the baseline. The results regarding the effect of rail size may be somewhat exaggerated in a practical sense, because a 70 ASCE rail section is considered to be a very light rail, especially when the traffic is assumed to primarily consist of fully loaded hopper cars. If the very light rail is excluded from the sensitivity studies, the effect of rail size on both safe crack-growth life and critical defect size is comparable to the effect of dynamic load factor. In general, the effect of foundation stiffness on the safe crack-growth life and critical defect size is weak compared to the other factors examined in the sensitivity studies.

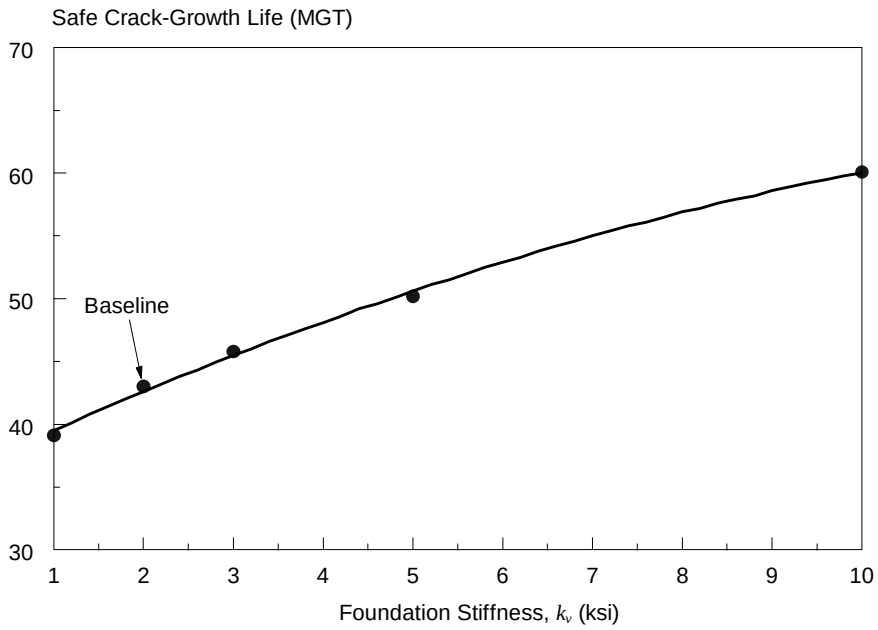

Figure 23. Effect of Foundation Stiffness on RDF Safe Crack-Growth Life

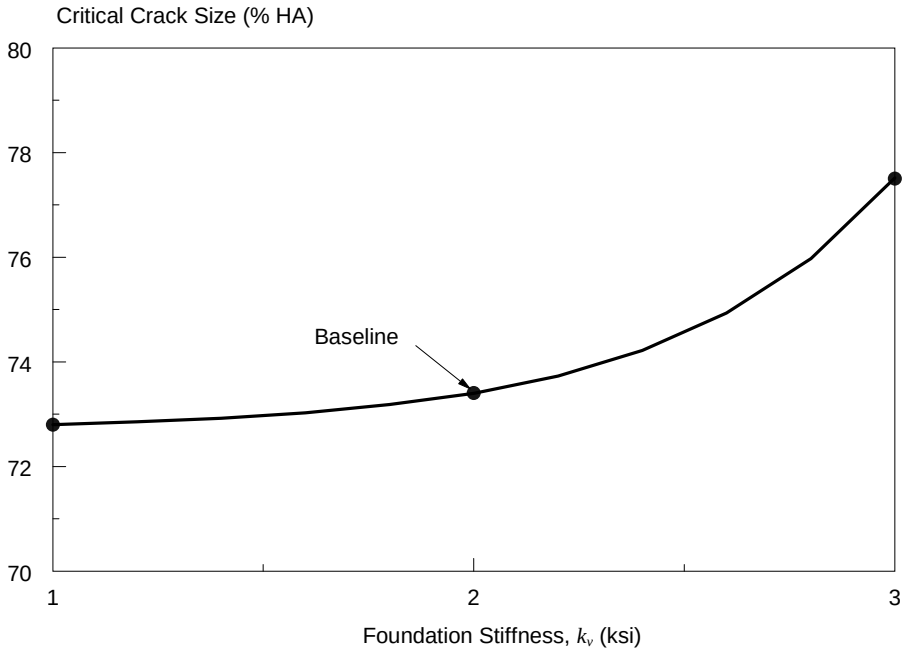

Figure 24. Effect of Foundation Stiffness on Critical RDF Size

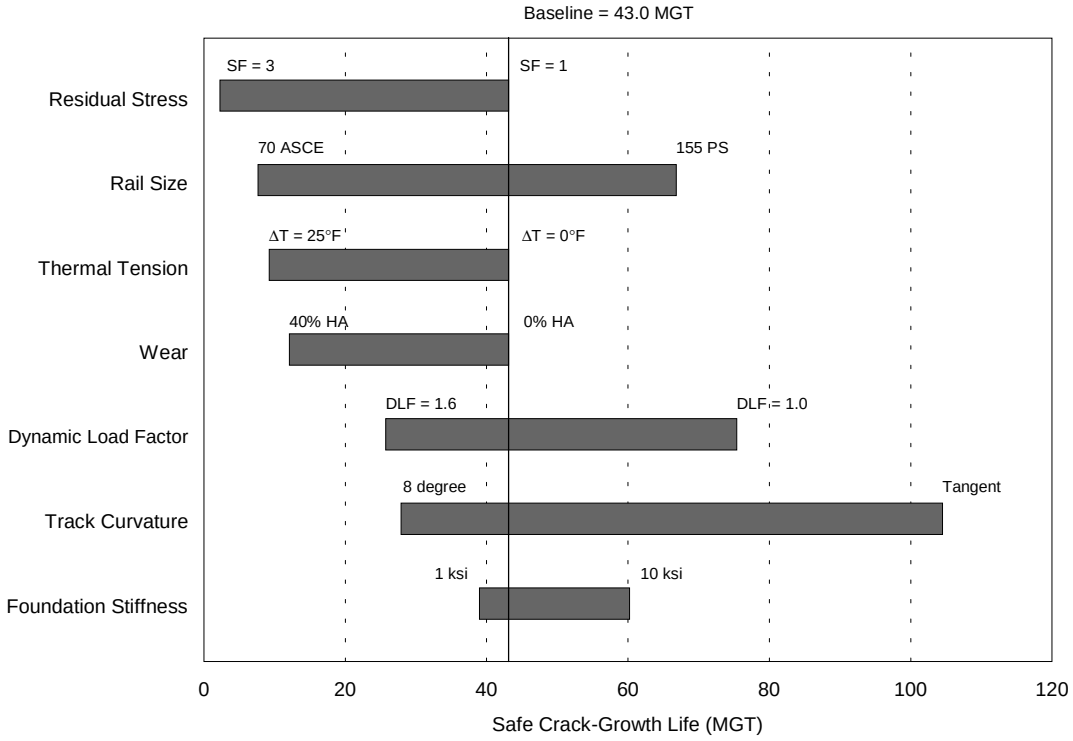

Figure 25. Summary of RDF Results for Safe Crack-Growth Life

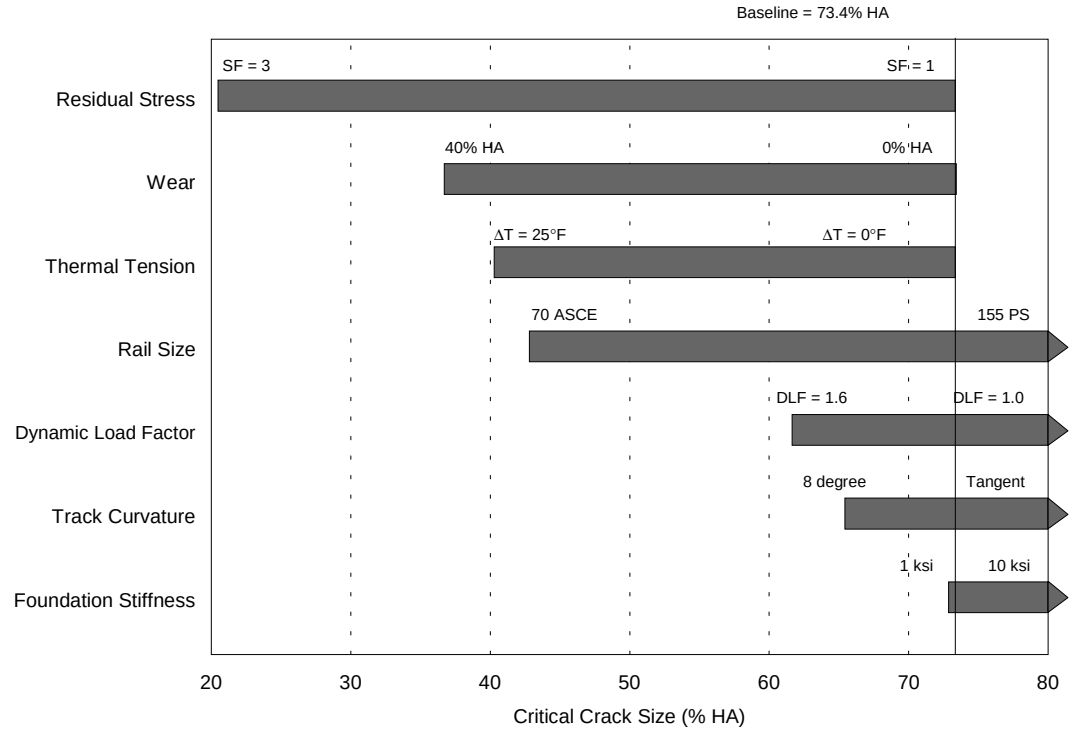

Figure 26. Summary of Results for Critical RDF Defect Sizes

3.9 COMPARISON WITH DETAIL FRACTURE

As described in the Introduction, detail fractures have been studied extensively in previous research efforts. Therefore, a comparison between the growth rates of DF and RDF defects seems logical. Figure 27 compares the crack-growth curves for a detail fracture (DF) and an RDF defect under baseline conditions. The RDF defect initially grows at a comparable rate to the DF, but its safe crack-growth life is roughly 20% shorter than the DF life. The critical size of the detail fracture under baseline conditions was found to be greater than 80% HA, compared to 73.4% HA for the RDF defect.

Another comparison between the growth rate of DF and RDF defects can be made by applying the worn rail analysis for head-height loss (as described in Section 2.4). The effect of wear in terms of head-height loss has not been examined in any of the previous studies involving detail fractures. The effect of rail-head height loss on the growth rate of detail fractures is shown in Figure 28. A 20% loss in rail-head height reduces the DF safe crack-growth life by almost 60% (from the baseline case of no wear); and a 40% loss reduces the safe life by over 80%. By comparison, the reduction in safe life for RDF defects was shown in Figure 12 to be over 40% for 20% head-height loss and more than 70% for 40% head-height loss. Thus, head-height loss has a greater influence on reducing the safe crack-growth life of detail fractures than on the safe life of RDF defects.

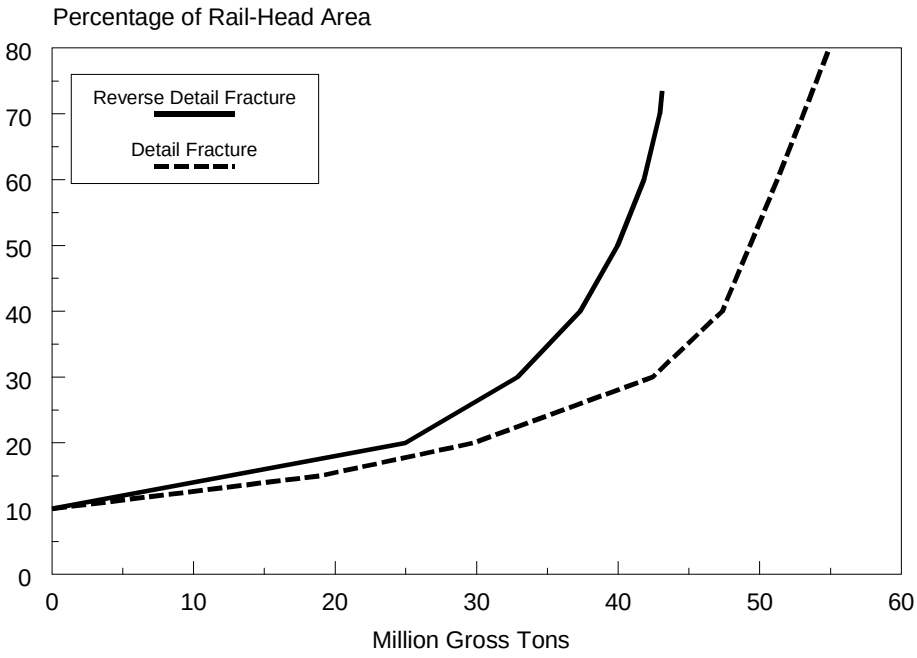

Figure 27. Comparison between DF and RDF Defect Growth

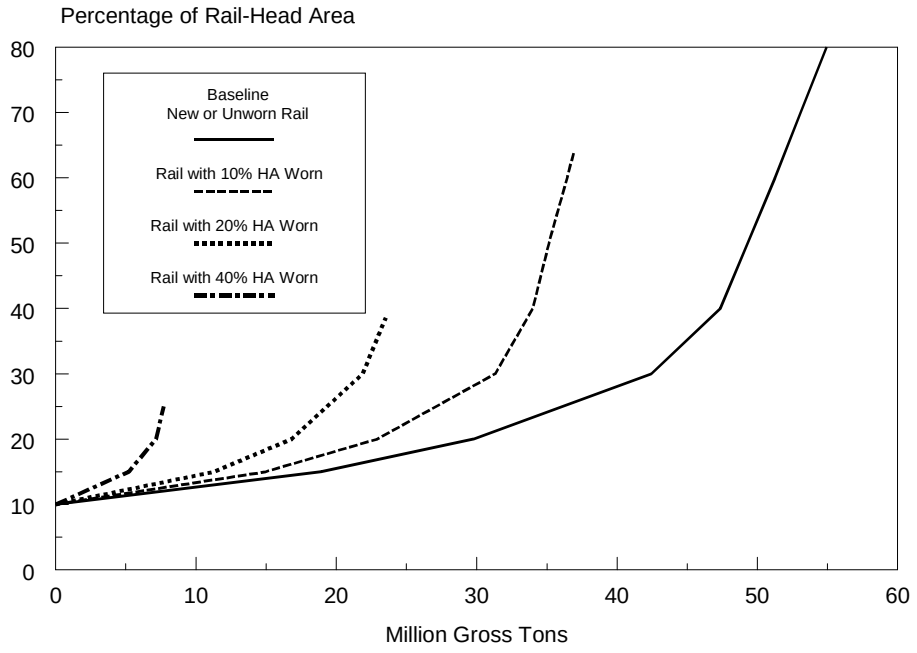

Figure 28. Effect of Head-Height Loss on DF Growth Rate

4. CONCLUSIONS

The following conclusions have been drawn based upon the results of analyses described and presented in this report.

1. The model indicates that RDF safe crack-growth life is comparable to, but somewhat shorter than, DF safe crack-growth life under the same conditions. Therefore, comparable or somewhat more frequent rail inspection is appropriate for areas where RDF defects are known to occur.

2. Residual stress, rail section, thermal tension, and rail wear have the strongest effect on reduction of RDF safe crack-growth life. These factors also have the greatest influence on reducing the critical RDF defect size, but in a different relative ranking order. Thus, the model results suggest that a doubling of rail inspection frequency should be considered, relative to the baseline, for light rail, worn rail with 20% head-height loss, or continuous welded rail in northern climates where the service temperature averages 10 to 25°F or more below the neutral temperature.

3. Track curvature has the most significant effect on the range of possible safe crack-growth lives that could be encountered in service. Safe life varies between 27.8 MGT on an 8-degree curve and 104.4 MGT for tangent track.

4. The effect of foundation stiffness on safe crack-growth life and critical RDF size is relatively weak compared to the influence of the other factors examined in these studies.

5. The effect of wear was examined by assuming two different wear patterns. One geometry assumed that material was worn directly off the top of rail, resulting in loss of head height. The other pattern assumed that material was worn from the gauge-side face. Safe crack-growth life for RDF defects was found to be shorter when loss of head height was assumed than when an equivalent level of wear (in percentage of head area) was assumed for reduced head width.

6. Loss of rail-head height has a greater influence on reducing the safe crack-growth life of detail fractures than on the safe life of RDF defects.

REFERENCES

1. Besuner, P.M. 1978. "Fracture Mechanics Analysis of Rails with Shell-Initiated Transverse Cracks" in *Rail Steels – Developments, Processing, and Use,* ASTM STP 644:303-329. American Society for Testing and Materials.

2. Orringer, O., J.M. Morris, and R.K. Steele. 1984. "Applied Research on Rail Fatigue and Fracture in the United States" in *Theoretical and Applied Fracture Mechanics* 1:23-49.

3. Sih, G.C., and D.Y. Tzou. 1984. "Three-Dimensional Transverse Fatigue Crack Growth in Rail Head" in *Theoretical and Applied Fracture Mechanics* 1:103-115.

4. Orringer, O., J.M. Morris, and D.Y. Jeong. 1986. "Detail Fracture Growth in Rails: Test Results" in *Theoretical and Applied Fracture Mechanics* 5:63-95.

5. Orringer, O., Y.H. Tang, J.E. Gordon, D.Y. Jeong, J.M. Morris, and A.B. Perlman. 1988. *Crack Propagation Life of Detail Fractures in Rail.* DOT/FRA/ORD-88/13. DOT-TSC-FRA-88-1. October 1988 Final Report.

6. Tada, H., P. Paris, and G. Irwin. 1985. *The Stress Analysis of Cracks Handbook.* 2nd edition, Paris Productions.

7. Rooke, D.P., and D.J. Cartwright. 1976. *Compendium of Stress Intensity Factors*. United Kingdom: HM Stationery Office.

8. Clayton, P., and Y.H. Tang. 1992. "Detail Fracture Growth in Curved Track at the Facility for Accelerated Service Testing" in *Residual Stresses in Rails* 1:37-56. The Netherlands: Kluwer Academic Publishers.

9. Timoshenko, S., and B.F. Langer. 1932. "Stresses in Railroad Track" in *ASME Transactions* 54:277-293.

10. Fata, R.G. 1996. Residual Stresses Resulting from Quench Hardening the Head of a Railroad Rail. M.S. Thesis, Department of Mechanical Engineering, Tufts University, Medford, MA.

11. Wineman, S.J. 1991. Residual Stresses and Web Fracture in Roller Straightened Rail. Ph.D. Thesis, Department of Mechanical Engineering, Massachusetts Institute of Technology, Cambridge, MA.

12. Orkisz, J., and A. Harris. 1988. "Analysis of Residual Stresses at Shakedown: a Hybrid Approach" in *Theoretical and Applied Fracture Mechanics* 9:109-121.

REFERENCES (continued)

13. Groom, J.J. 1983. *Determination of Residual Stresses in Rails*. DOT/FRA/ORD-83/05, DOT-TSC-FRA-81-21. May 1983 Final Report.

14. Shah, R.C., and A.S. Kobayashi. 1971. "Stress Intensity Factor for an Elliptical Crack under Arbitrary Normal Loading" in *Engineering Fracture Mechanics* 3:71-96.

15. Walker, E.K. 1970. "The Effect of Stress Ratio During Crack Propagation and Fatigue for 2024-T3 and 7075-T6 Aluminum" in *Effects of Environment and Complex Load History on Fatigue Life*. ASTM STP 462:1-14. American Society for Testing and Materials.

16. Newman, J.C., Jr., and W. Elber (Editors). 1988. *Mechanics of Crack Closure*. ASTM STP 982. Philadelphia: American Society for Testing and Materials.

17. Orringer, O. 1984. "Rapid Estimation of Spectrum Crack Growth Life Based on the Palmgren-Miner Rule" in *Computers & Structures* 19:149-153.

18. Sih, G.C., and D.Y. Jeong. 1992. "Effect of load sequence on fatigue life of rail steel" in *Residual Stresses in Rails*. Vol. 2, The Netherlands: Kluwer Academic Publishers, 63-85.

19. McGee, G.M. 1965. *Calculations of Rail Bending Stress for 125 Ton Tank Cars*. Chicago: AAR Research Center. Report No. 19506, April 1965.

20. Srinvasan, M. 1969. *Modern Permanent Way*. Bombay: Smaiya Publications, 134-136.

APPENDIX A. EQUATIONS FOR RAIL-BENDING STRESSES

The longitudinal bending stresses in the rail-head comprise five components: (1) vertical bending, (2) lateral bending, (3) vertical head-on-web bending, (4) lateral head-on-web bending, and (5) warping. The total longitudinal bending stress at a given point in the rail head is simply the sum of these five components. The equations to determine these individual stress components are listed in this appendix.

Vertical Bending

The dominant bending stress component is due to the vertical wheel loading

$$\sigma_V = \frac{M_v(x) z_1}{I_{yy}} \tag{A.1}$$

where

$$z_1 = h_{TOT} - z_N - z^* \tag{A.2}$$

where h_{TOT} is the total height of the rail, z_N is the distance from the bottom of the rail to the rail neutral axis, and z^* is the distance from the top of the unworn rail crown to the stress point. Dimensions for a generic rail section are shown in Figure A-1. The vertical bending moment is given by

$$M_V(x) = -\sum_i \frac{V_i}{4\beta_V} e^{-\beta_V |x-\xi_i|} \left[\cos\beta_V (x-\xi_i) - \sin\beta_V |x-\xi_i| \right] \tag{A.3}$$

In this equation, $1/\beta_V$ is the characteristic wavelength, which is determined from

$$\beta_V = \sqrt[4]{\frac{k_V}{4EI_{yy}}} \tag{A.4}$$

where k_V is the vertical foundation stiffness, E is the modulus of elasticity for rail steel (assumed to be 30×10^6 psi), and I_{yy} is the second area moment of inertia about the horizontal axis through the centroid of the entire rail. The summation is performed over the number of wheel loads, where V_i is the magnitude of the i^{th} vertical wheel load and ξ_i is the position of the i^{th} wheel load relative to x.

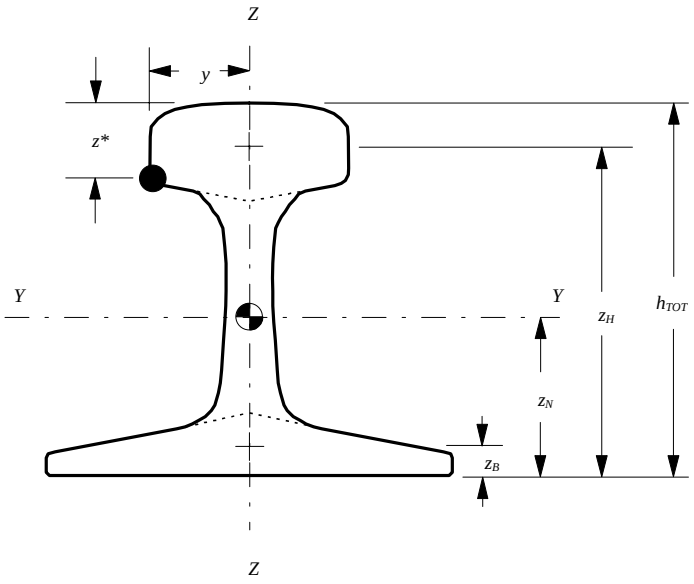

Figure A-1. Dimensions for a Generic Rail Section

Lateral Bending

The bending stress component due to lateral loading is

$$\sigma_L = \frac{M_L(x)y}{I_{zz}} \tag{A.5}$$

The lateral bending moment is defined by the following function

$$M_L(x) = -\sum_i \frac{L_i}{4\beta_L} e^{-\beta_L|x-\xi_i|}\left[\cos\beta_L(x-\xi_i) - \sin\beta_L|x-\xi_i|\right] \tag{A.6}$$

where the characteristic wavelength for lateral bending, $1/\beta_L$, is defined from

$$\beta_L = \sqrt[4]{\frac{k_L}{4EI_{zz}}} \tag{A.7}$$

In this equation, k_L is the lateral foundation stiffness (the RDF defect model assumes that k_L =0.85 k_v), I_{zz} is the second area moment of inertia about the vertical axis through the centroid of the entire rail, and L_i is the magnitude of the $i^{\underline{th}}$ lateral wheel load.

Vertical Head-on-Web Bending

The rail head can be assumed to behave as a beam supported by an elastic foundation formed by the rail web. This additional vertical bending component is calculated from

$$\sigma_{V_{how}} = \frac{M_{V_{how}}(x) z_2}{I_{yyH}} \tag{A.8}$$

The distance from the neutral axis of the rail head to the stress point is

$$z_2 = h_{TOT} - z_H - z^* \tag{A.9}$$

where z_H is the distance from the bottom of the rail to the neutral axis of the rail head. The vertical head-on-web bending moment is given by

$$M_{V_{how}}(x) = -\sum_i \frac{V_i}{4\beta_{V_{how}}} e^{-\beta_{V_{how}}|x-\xi_i|}\left[\cos\beta_{V_{how}}(x-\xi_i) - \sin\beta_{V_{how}}|x-\xi_i|\right] \tag{A.10}$$

and

$$\beta_{V_{how}} = \sqrt[4]{\frac{k_{V_{how}}}{4EI_{yyH}}} \tag{A.11}$$

where I_{yyH} is the second area moment of inertia for the rail head only with respect to the horizontal axis through the centroid of the head. The effective vertical head-on-web stiffness is defined by Timoshenko and Langer [9] as

$$k_{V_{how}} = E\left(\frac{t_w}{h_w}\right) \tag{A.12}$$

where t_w is the average web thickness, and h_w is the height of the rail web.

Lateral Head-on-Web Bending

The lateral head-on-web bending stress is calculated from

$$\sigma_{L_{how}} = \frac{M_{L_{how}}(x) y}{I_{zzH}} \tag{A.13}$$

The lateral head-on-web bending moment is given by

$$M_{L_{how}}(x) = -\sum_i \frac{L_i}{4\beta_{L_{how}}} e^{-\beta_{L_{how}}|x-\xi_i|}\left[\cos\beta_{L_{how}}(x-\xi_i) - \sin\beta_{L_{how}}|x-\xi_i|\right] \quad \text{(A.14)}$$

and

$$\beta_{L_{how}} = \sqrt[4]{\frac{k_{L_{how}}}{4EI_{zzH}}} \quad \text{(A.15)}$$

where I_{zzH} is the second area moment of inertia for the rail head only with respect to the vertical axis through the centroid of the head. The effective lateral head-on-web stiffness is defined by Timoshenko and Langer [9] as

$$k_{L_{how}} = E\left(\frac{t_w}{h_w}\right)^3 \quad \text{(A.16)}$$

Warping

Eccentric vertical wheel loading (i.e., vertical loads not applied directly at the vertical centerline of the rail) and lateral wheel loading cause the rail to twist. The warping component of the longitudinal bending stress is related to the second derivative of the angle of twist by

$$\sigma_W = Eh_1 y \frac{d^2\phi}{dx^2} \quad \text{(A.17)}$$

where ϕ is the angle of twist, and h_1 is the distance between the centroid of the head and the shear center of the entire rail, which is determined

$$h_1 = h\frac{I_{zzB}}{I_{zzH} + I_{zzB}} \quad \text{(A.18)}$$

In this equation, I_{zzH} and I_{zzB} are the second area moments for lateral bending of the head and base of the rail, and h is the distance between the centroids of the head and base

$$h = z_H - z_B \quad \text{(A.19)}$$

where z_B is the distance from the bottom of the rail to the centroid of the base only. The second derivative of the angle of twist is defined as

$$\frac{d^2\phi}{dx^2} = \sum_i \frac{L_i f - V_i e}{4Dh^2\beta_1\beta_2}\left[\beta_1 \sinh\beta_2(x-\xi_i) - \beta_2 \cosh\beta_2|x-\xi_i|\right] \quad \text{(A.20)}$$

where f is the distance between the lateral load and the shear center, and e is the distance between the vertical load and the shear center (see Figure A-2).

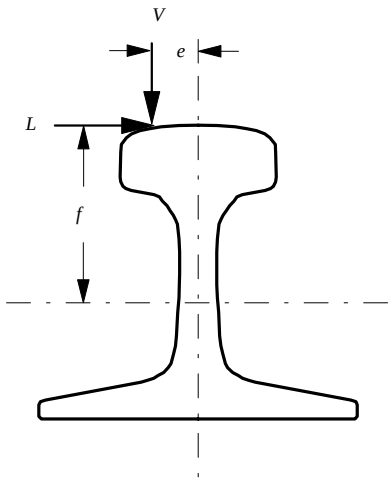

Figure A-2. Eccentric Vertical Loading and Lateral Loading of Rail

The auxiliary functions are defined as

$$\beta_1 = \sqrt{\frac{C}{4Dh^2} + \lambda^2} \qquad \beta_2 = \sqrt{\frac{C}{4Dh^2} - \lambda^2} \quad \text{(A.21)}$$

$$\lambda = \sqrt[4]{\frac{k_t}{4Dh^2}} \quad \text{(A.22)}$$

where k_t is the torsional foundation stiffness (assumed to be 10^5 lb-in/rad-in). In addition, D is called the warping constant (in units of lb-in^2), and is defined as

$$D = E\,\frac{I_{zzB} I_{zzH}}{I_{zzB} + I_{zzH}} \quad \text{(A.23)}$$

and C is called the torsion constant (in units of lb-in^2)

$$C = \frac{GA_R^4}{40J_c} \quad \text{(A.24)}$$

where G is the shear modulus of elasticity, and A_R is the cross-sectional area of the entire rail section. The shear modulus is defined as $G=E/2(1+\nu)$, where ν is Poisson's ratio for rail steel (assumed to be 0.3). Equation (A.24) also depends on J_c , the polar moment of inertia with respect to the shear center, which is defined as

$$J_c = J_o + A_R(z_N - z_c)^2 \tag{A.25}$$

where J_o is the polar moment of inertia with respect to the centroid

$$J_o = I_{yy} + I_{zz} \tag{A.26}$$

and z_c is the distance from the bottom of the rail to the shear center or center of twist

$$z_c = z_B + (z_H - z_B)\frac{I_{zzH}}{I_{zzB} + I_{zzH}} \tag{A.27}$$

APPENDIX B. EQUATIONS FOR SECTION PROPERTIES OF WORN RAIL

Two types of worn rail-head geometry were considered in this report: a uniform loss of head height directly off the top of the rail, and a uniform loss of head width from the gage-side face. As described in Section 2.4, the analysis of worn rail assumes that the rail head cross-section is rectangular. The equations to calculate rail section properties of worn rail, based on this simplifying assumption, are listed in this appendix. These section properties are required in the stress analysis described in Appendix A.

Loss of Rail Head Height

For worn rail with loss of rail-head height, the area moments of inertia for both vertical and lateral bending of the worn rail are determined by decreasing the height by the same percentage as that for rail-head area worn. The vertical and lateral bending inertias as functions of wear are defined, respectively, as

$$I_{yyH}(X) = \frac{1}{12} \cdot \left[\left(\frac{100 - X}{100} \right) \cdot h_{eq} \right]^3 \cdot w_{eq} \tag{B.1}$$

and

$$I_{zzH}(X) = \frac{1}{12} \cdot \left[\left(\frac{100 - X}{100} \right) \cdot h_{eq} \right] \cdot {w_{eq}}^3 \tag{B.2}$$

where h_{eq} is the equivalent rail-head height, w_{eq} is the equivalent rail-head width, and X is a variable quantifying wear in terms of percentage of rail-head area (i.e., $0 \le X \le 100$). The equivalent rail-head height and width were defined in equations (17) and (18), respectively.

The derivation of the equation to calculate the vertical bending inertia for the entire worn rail was described briefly in Section 2.4. Referring to Figure 7, the following expression was derived from equation (20)

$$\begin{aligned} I_{yy}(X) = I_{Y'Y'} + A_R \cdot \left[z_N(0) - z_N(X) \right]^2 - \frac{1}{12} \cdot \left(\frac{X}{100} \cdot h_{eq} \right)^3 \cdot w_{eq} \cdots \\ - \left[\left(\frac{X}{100} \cdot h_{eq} \right) \cdot w_{eq} \right] \cdot \left[h_{TOT} - \frac{1}{2} \cdot \left(\frac{X}{100} \cdot h_{eq} \right) - z_N(X) \right]^2 \end{aligned} \tag{B.3}$$

where $I_{Y'Y'}$ is the vertical bending inertia for the entire unworn or new rail, h_{TOT} is the total height of the unworn or new rail, A_R is the cross-sectional area of the unworn rail, $z_N(0)$ refers to the location of the centroid for the unworn rail, and $z_N(X)$ is the location of the

centroid for the worn rail. The lateral bending inertia for the entire worn rail is calculated from

$$I_{zz}(X) = I_{zzH}(X) + I_{zzW} + I_{zzB} \tag{B.4}$$

where I_{zzW} are I_{zzB} are lateral bending inertias for the rail web and rail base, respectively.

For a rail with loss of head height, the centroid of the head only and the centroid of the entire rail are located along the the vertical centerline of the rail, since it is also a line of symmetry. The vertical distance from the bottom of a worn rail to the centroid of the head is estimated by

$$z_H(X) = h_{TOT} - \frac{1}{2} \cdot \left(\frac{X}{100} \cdot h_{eq} \right) \tag{B.5}$$

The distance from the bottom of the rail to the centroid of the entire worn rail is

$$z_N(X) = \frac{A_B \cdot z_B + A_W \cdot z_W + \left[\left(\frac{100 - X}{100} \right) \cdot A_H \right] \cdot z_H(X)}{A_B + A_W + \left[\left(\frac{100 - X}{100} \right) \cdot A_H \right]} \tag{B.6}$$

where A_B is the cross-sectional area of the rail base, A_W is the cross-sectional area of the rail web, A_H is the cross-sectional area of the unworn or new rail head, z_B is the distance from the bottom of the rail to the centroid of the base only, and z_W is the distance from the bottom of the rail to the centroid of the web only.

Loss of Rail Head Width

For worn rail with loss of rail-head width from the gage-side face, the area moments of inertia for both vertical and lateral bending are determined by decreasing the rail-head width by the same percentage as that for rail-head area worn. The vertical and lateral bending inertias for a worn rail head are defined, respectively, as

$$I_{yyH}(X) = \frac{1}{12} \cdot {h_{eq}}^3 \cdot \left(\frac{100 - X}{100} \right) w_{eq} \tag{B.7}$$

and

$$I_{zzH}(X) = \frac{1}{12} \cdot h_{eq} \cdot \left[\left(\frac{100 - X}{100} \right) \cdot w_{eq} \right]^3 \tag{B.8}$$

Derivations of the equations to calculate the second area moments of inertia for the entire worn rail in vertical and lateral bending were described briefly in Section 2.4. Referring to Figure 8, equation (21) is equivalent to

$$I_{zz}(X) = I_{Z'Z'} + A_R \cdot y_N(X)^2 - \frac{1}{12} \cdot h_{eq} \cdot \left(\frac{X}{100} w_{eq}\right)^3 \cdots - \left[h_{eq} \cdot \left(\frac{X}{100} \cdot w_{eq}\right)\right] \cdot \left[\frac{1}{2} \cdot w_{eq} \cdot \left(1 - \frac{X}{100}\right) + y_N(X)\right]^2 \quad \text{(B.9)}$$

where $I_{Z'Z'}$ is the lateral bending inertia for the entire unworn or new rail. Referring to Figure 9, equation (22) is equivalent to

$$I_{yy}(X) = I_{Y'Y'} + A_R \cdot \left[z_N(0) - z_N(X)\right]^2 - \frac{1}{12} \cdot {h_{eq}}^3 \cdot \left(\frac{X}{100} w_{eq}\right) \cdots - \left[h_{eq} \cdot \left(\frac{X}{100} w_{eq}\right)\right] \cdot \left[h_{TOT} - \frac{1}{2} \cdot h_{eq} - z_N(X)\right]^2 \quad \text{(B.10)}$$

Wear from the gage-side face results in an asymmetric rail cross-section with respect to the vertical midplane. Therefore, the locations of the centroids for the worn rail head only and for the entire worn rail are offset from the vertical midplane of the unworn or new rail (see Figure B.1). The horizontal distance of the rail-head centroid to the vertical centerline of the unworn rail is defined as

$$y_H(X) = \frac{1}{2} \cdot \left(\frac{X}{100} \cdot w_{eq}\right) \quad \text{(B.11)}$$

The vertical location of the rail head centroid at the bottom of the worn rail is unchanged from the location for an unworn rail.

For the entire worn rail, the location of the centroid is defined by

$$y_N(X) = \frac{\left[\left(\frac{100 - X}{100}\right) \cdot A_H\right] \cdot y_H(X)}{A_B + A_W + \left[\left(\frac{100 - X}{100}\right) \cdot A_H\right]} \quad \text{(B.12)}$$

which is the horizontal distance from the midplane of the unworn rail, and by

$$z_N(X) = \frac{A_B \cdot z_B + A_W \cdot z_W + \left[\left(\frac{100 - X}{100}\right) \cdot A_H\right] \cdot z_H}{A_B + A_W + \left[\left(\frac{100 - X}{100}\right) \cdot A_H\right]} \tag{B.13}$$

which is the vertical distance from the bottom of the rail.

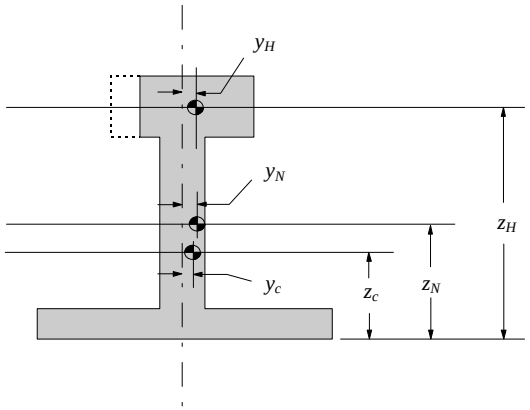

Figure B-1. Shear Center and Centroid Locations for Rail with Reduced Head Width

Additional Section Properties Affected by Wear

In addition to the section properties described in equations (B.1) to (B.13), wear affects other rail section properties that are required in the stress analysis described in Appendix A. These other section properties may depend upon the area moments of inertia and the centroids for a worn rail as defined by these previous equations.

The horizontal distance from the shear center or center of twist for the entire worn rail to the midplane of the unworn rail (Figure B.1) is

$$y_c(X) = y_H(X) \cdot \frac{I_{yyH}(X)}{I_{yyB} + I_{yyH}(X)} \tag{B.14}$$

where I_{yyB} is the vertical bending inertia for the rail base only. For the case of head-height loss, the shear center and the centroid of the rail head only are located along the vertical centerline of the unworn rail; in other words, y_c and y_H are equal to zero. The vertical distance of the shear center to the bottom of the rail is given by

$$z_c = z_B + \left[z_H(X) - z_B\right] \cdot \frac{I_{zzH}(X)}{I_{zzB} + I_{zzH}(X)} \tag{B.15}$$

The polar moment of inertia of the worn rail with respect to the shear center as a function of wear (i.e., either loss of rail-head height or width) is defined as

$$J_c(X) = J_o(X) + \left[A_B + A_W + \left(\frac{100 - X}{100} \right) \cdot A_H \right] \cdot \left[(z_N(X) - z_c(X))^2 + (y_N(X) - y_c(X))^2 \right] \quad \text{(B.16)}$$

where

$$J_o(X) = I_{yy}(X) + I_{zz}(X) \quad \text{(B.17)}$$

is the polar moment of inertia with respect to the centroid of the entire worn rail.

The torsion constant as a function of wear is calculated from

$$C(X) = \frac{G \cdot \left[A_B + A_W + \left(\frac{100 - X}{100} \right) \cdot A_H \right]^4}{40 \cdot J_c(X)} \quad \text{(B.18)}$$

where G is the shear modulus for rail steel.

The warping constant is also affected by rail wear, and is determined from

$$D(X) = E \cdot \frac{I_{zzB} \cdot I_{zzH}(X)}{I_{zzB} + I_{zzH}(X)} \quad \text{(B.19)}$$

where E is the modulus of elasticity.

From geometric considerations, the distance between centroids of the worn head and the rail base is calculated from

$$h(X) = \sqrt{y_H(X)^2 + \left[z_H(X) - z_B \right]^2} \quad \text{(B.20)}$$

This equation is needed to calculate the distance between the centroid of the worn rail head and the center of twist

$$h_1(X) = h(X) \cdot \frac{I_{zzB}}{I_{zzH}(X) + I_{zzB}} \quad \text{(B.21)}$$